

---

# SPURIOUS RECONSTRUCTION FROM BRAIN ACTIVITY

---

A PREPRINT

Ken Shirakawa<sup>\*1,2</sup>, Yoshihiro Nagano<sup>1,2</sup>, Misato Tanaka<sup>1,2</sup>, Shuntaro C. Aoki<sup>1,2</sup>, Kei Majima<sup>3</sup>, Yusuke Muraki<sup>1</sup>,  
and Yukiyasu Kamitani<sup>\*1,2</sup>

<sup>1</sup>Graduate School of Informatics, Kyoto University, Kyoto, Japan

<sup>2</sup>Department of Neuroinformatics, ATR Computational Neuroscience Laboratories, Kyoto, Japan

<sup>3</sup>National Institutes for Quantum Science and Technology, Chiba, Japan

## ABSTRACT

The rapid advances in brain decoding, particularly visual image reconstruction, have sparked discussions about the potential societal implications and ethical considerations surrounding neurotechnology. As these methods aim to recover perceived images from brain activity and achieve prediction over diverse images beyond training samples (zero-shot prediction), it is crucial to critically assess their capabilities and limitations to prevent misguided public expectations and inform future regulations. Our case study of recent text-guided reconstruction methods, which leverage a large-scale dataset (the Natural Scene Dataset, NSD) and text-to-image diffusion models, reveals significant limitations in their generalizability. We found a notable decrease in performance when applying these methods to a different dataset, which was designed to prevent category overlaps between training and test sets. UMAP visualization of the text features with NSD images showed a limited diversity of distinct semantic and visual clusters, with substantial overlap between training and test sets. Formal analysis and simulations demonstrated that clustered training samples can lead to “output dimension collapse,” restricting the output feature dimensions predictable from brain activity. Diversifying the training set to ensure a broader feature distribution improved generalizability beyond the trained clusters. However, text features alone are insufficient for a complete mapping to the visual space, even if perfectly predicted from brain activity. We argue that recent photo-like reconstructions may primarily be a blend of classification into trained categories and the generation of convincing yet inauthentic images through text-to-image diffusion (hallucination). To achieve genuine zero-shot prediction, diverse datasets and compositional representations spanning the image space are essential. As neurotechnology advances, engaging in interdisciplinary discussions involving neuroscientists, ethicists, policymakers, and the public is crucial to ensure responsible development and application of these techniques. These discussions should be grounded in a clear understanding of the current capabilities and limitations of the technology, as well as a careful consideration of the potential ethical and societal impacts.

**Keywords** Visual image reconstruction · brain decoding · zero-shot prediction · methodology · generative AIs

## 1 Introduction

Brain decoding has been widely used in the neuroscience field, revealing specific contents of the mind (Haxby et al., 2001; Kamitani and Tong, 2005; Soon et al., 2008; Horikawa et al., 2013). As brain decoding is sometimes referred to as “mind-reading” in popular media (Somers, 2021; Whang, 2023; Raasch, 2023), it has attracted significant attention beyond the scientific community due to its potential for real-world applications in medicine and industry. Such neurotechnology has also started to affect future ethical discussions and legal regulations (UNESCO, 2023). To prevent misleading public expectations and policies, scientists need to carefully assess the current status of brain decoding techniques and clarify the possibilities and limitations.

---

<sup>\*</sup>Corresponding author: Ken Shirakawa (shirakawaken0118@gmail.com) and Yukiyasu Kamitani (kamitani@i.kyoto-u.ac.jp)

One of the major challenges in brain decoding is the limited amount of brain data we can collect. The current brain measurement devices are costly, yielding far less brain data than the amounts typically used in image or text processing within the field of computer science and AI (Deng et al., 2009; Schuhmann et al., 2022). Although we have gradually increased the amount of brain data per subject (Van Essen et al., 2012; Allen et al., 2022; Naselaris et al., 2021; Hebart et al., 2023; Xu et al., 2024), it remains impractical to collect brain data covering the full range of cognitive states and perceptual experiences. Consequently, classification-based decoding approaches, primarily developed in the early stages of this field, are insufficient to uncover the neural code in general or natural conditions since decodable information is confined to the same stimuli or predefined categories used in a training phase.

To overcome this limitation, several decoding methods have been proposed to enable the prediction of novel contents from brain activities that are not encountered during the training phase. Kay et al. (2008) proposed a general visual decoding approach via a statistical encoding model that predicted fMRI voxel values from image features. It successfully identified novel test images from a set of 1000 candidates. Mitchell et al. (2008) utilized co-occurrence rates of specific verb sets for nouns to predict fMRI brain activity during the perception of line drawing images, demonstrating the ability to predict unseen nouns. Brouwer and Heeger (2009) constructed a color-tuning model and predicted brain activity while the subjects were presented with color stimuli. As their training stimuli cover most of the color space, their methods can successfully identify novel colors not included in the training dataset. Horikawa and Kamitani (2017) utilized deep neural network (DNN) features to decode brain activity measured while subjects perceived natural images. They showed successful prediction of novel object categories not encountered during the training phase.

In the field of machine learning, “zero-shot” prediction refers to the ability of a model to accurately predict or classify novel contents that were not encountered during the training phase (Larochelle et al., 2008; Palatucci et al., 2009). This technique has found widespread application across various domains, including image classification (Radford et al., 2021), image generation (Ramesh et al., 2021), and natural language processing (Brown et al., 2020). The concept of zero-shot prediction can be considered analogous to brain decoding techniques that aim to interpret brain activity patterns associated with previously unseen stimuli or experiences. Both approaches seek to generalize knowledge gained from a limited set of training data to novel situations, enabling the interpretation of new information without explicit prior exposure. To achieve effective zero-shot prediction, the model often utilizes a compositional representation of the output (Lake et al., 2017; Higgins et al., 2018). Compositional representation refers to the ability to understand and generate novel combinations of previously learned concepts or features. By learning the underlying structure and relationships between different elements, the model can generalize its knowledge to new, unseen instances.

Visual image reconstruction is another prominent example of zero-shot prediction in brain decoding. This task aims to recover perceived novel images that were not encountered during the training phase, effectively reconstructing visual experiences from brain activity patterns (Stanley et al., 1999; Miyawaki et al., 2008). As our perceptual visual experiences cannot be fully covered by limited brain data, reconstruction methods require strong generalizability. Miyawaki et al. (2008) conducted a study that demonstrated the reconstruction of perceived arbitrary 10x10 binary-contrast images from brain activity. They built multiple modular decoders to predict the local contrasts of each location and combined their predictions. This approach leverages the compositional representation of the visual field, which is organized retinotopically in the early visual cortex. Incorporating cortical organization into the model’s architecture can significantly improve its ability to perform zero-shot prediction and reconstruct novel visual experiences from brain activity. Although the training stimuli were only 400 random images, it was possible to reconstruct an arbitrary image from a set of possible  $2^{100}$  instances, including geometric shapes such as crosses and alphabets. Similarly, Shen et al. (2019b) replaced local decoders with DNN feature decoders. Although their training stimuli were 1200 natural images, they demonstrated reconstructing novel images, including artificial images, which were not part of the training set. These successes suggest that the proposed reconstruction models capture rich and comprehensive information about the general aspects of the neural code, beyond merely the information defined by the training data (Kriegeskorte and Douglas, 2019). Developing reliable reconstruction methods also enables further analysis of subjective visual experiences, such as visual imagery (Shen et al., 2019b), attention (Horikawa and Kamitani, 2022), and illusion (Cheng et al., 2023). Enabling the decoding of novel brain states that were never encountered during the training phase can be a promising approach to neural mind-reading (Kamitani and Tong, 2005).

Visual image reconstruction pipelines can be divided into three main components: translator, latent features, and generator (Figure 1). The translator serves to convert a brain activity pattern into a latent feature space via linear regression (Shen et al., 2019b; Seeliger et al., 2018; Mozafari et al., 2020; Ozcelik et al., 2022; Kavasidis et al., 2017), or nonlinear transformation (Qiao et al., 2020). Latent features serve as surrogate representations of perceived visual images. While the local contrasts in Miyawaki et al. (2008) can be seen as a primitive form of latent features, recent studies often use DNN features, such as the intermediate output of recognition models (Shen et al., 2019b; Cheng et al., 2023). The generator visualizes translated latent features into images. Some studies have used the pretraining image generative models for the generator module (Mozafari et al., 2020; Qiao et al., 2020; Ozcelik et al., 2022; Kavasidis et al., 2017). Image optimization can also be regarded as a generator (Shen et al., 2019b). Direct mapping from brain



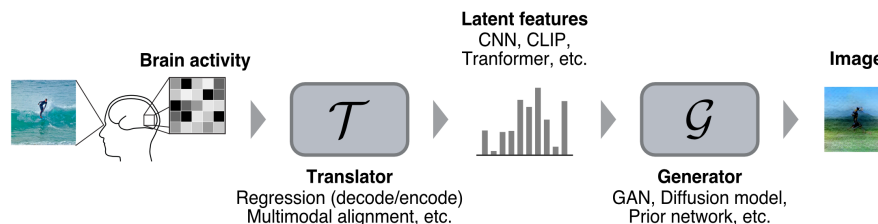


Figure 1: An overview of the visual image reconstruction pipeline. Brain activity recorded while perceiving a visual image is fed into a translator module. The translator maps the brain activity to latent features. The generator module converts the latent features into an image corresponding to the original visual stimulus.

activity to images using DNNs can also be considered to implicitly contain these components (Shen et al., 2019a; Belyi et al., 2019; Ren et al., 2021; Gaziv et al., 2022; Lin et al., 2022; Chen et al., 2023a).

Recent advances in generative AI, particularly in text-to-image generation, have naturally given rise to expectations that these techniques could provide a shortcut for visual image reconstruction by leveraging semantic representations. In addition, there has been a growing trend towards collecting neural datasets using a wide range of diverse visual and semantic content. This shift aims to capture a more comprehensive and ecologically valid representation of the human experience (Naselaris et al., 2021). Researchers have started to collect large-scale datasets, such as the Natural Scene Dataset (NSD) (Allen et al., 2022) and the THINGS-fMRI dataset (Hebart et al., 2023), which incorporate a broader range of fMRI data induced by diverse visual stimuli with text or category annotations. Notably, recent studies leveraging the latest generative AI techniques with semantic representation and large-scale datasets have reported photo-like reconstructions from brain activity (Takagi and Nishimoto, 2023b; Ozcelik and VanRullen, 2023; Scotti et al., 2023; Bai et al., 2023; Chen et al., 2023b; Lan et al., 2023; Benchetrit et al., 2024). They utilized contrastive language-image pretraining (CLIP) features (Radford et al., 2021) as latent features and text-to-image diffusion models (Ramesh et al., 2021; Xu et al., 2022) as generators.

While these recent approaches show promising results, it remains uncertain whether these methods truly achieve zero-shot reconstruction due to several factors. The complex model architectures employed in these studies, along with the use of a large-scale dataset, make it challenging to interpret and understand the underlying mechanisms driving the reconstruction process. To fully assess the zero-shot prediction capabilities of these approaches, it is essential to rigorously test their generalizability across different datasets and to provide detailed analyses of the individual model components. This includes evaluating the performance of the translators, latent features, and generators used in these methods. Furthermore, the characterization of the diversity of stimuli in the datasets and the latent representations has not been thoroughly explored. It is unclear whether the recently proposed datasets, such as the NSD, are optimally designed to capture the full range of human visual experiences and to support the development of truly generalizable prediction models.

In the following, we begin with a case study that critically tests the methods proposed by Takagi and Nishimoto (2023b) and Ozcelik and VanRullen (2023), which originally used the NSD. Our findings reveal several issues, including the failure of replication with another dataset specifically designed to avoid overlap between training and test sets (Shen et al., 2019b), and the questionable post-hoc selection procedures of Takagi and Nishimoto (2023b) that can produce convincing reconstructions even with random brain data. We identify the lack of diversity represented by the limited number of clusters in the NSD dataset as a potential factor contributing to these issues. We also demonstrate the failure of zero-shot prediction in the feature space and the inability to recover a stimulus from its latent features, suggesting a misspecification of the model. Based on these findings, we conclude that the apparent photo-like reconstructions are essentially a result of classification to clusters shared between training and test sets, combined with hallucinations by the generative model.

In the formal analysis and simulation section, we aim to uncover the general factors underlying the issues and observations highlighted in the case study. We first describe the phenomenon of “output dimension collapse” in the translation from brain activity to the latent feature space. We show that the regression model trained on the clustered outputs becomes specialized to the training examples and its output collapses into a subspace of the training dataset. Our simulations with clustered data demonstrate that out-of-sample prediction can be achieved with an increasing number of training clusters, suggesting that zero-shot prediction is possible if stimulus diversity and a compositional representation are available. We also explore the preservation of image information at hierarchical layers of DNNs and

discuss the caveats associated with evaluating reconstructions using identification metrics alone. Finally, we provide speculation on how we are fooled by the seemingly realistic reconstructions generated by AI models.

We conclude with recommendations for critically testing reconstruction models. Our findings highlight the importance of rigorous evaluation, the use of diverse datasets, and the need for careful specification and characterization of model components to advance the field of visual image reconstruction and develop truly generalizable prediction capabilities.

## 2 Results

### 2.1 Case study

We investigated two types of recent generative AI-based reconstruction methods, StableDiffusionReconstruction (Takagi and Nishimoto, 2023b) and Brain-diffuser (Ozcelik and VanRullen, 2023), as well as their validation dataset, the NSD (Allen et al., 2022). Both reconstruction methods utilize CLIP features (Radford et al., 2021) to effectively apply recent text-to-image diffusion models in visual image reconstruction analysis. CLIP text features are obtained from the average of five text annotations corresponding to the stimulus image. These text annotation information are only used during training to map the brain activity into CLIP text features. In the test phase, they directly predict CLIP text features from brain activity during image perception. Henceforth, these two reconstruction methods will be referred to together as text-guided reconstruction methods.

The StableDiffusionReconstruction method (Takagi and Nishimoto, 2023b) uses the components of the Stable Diffusion model (Ramesh et al., 2021), the VAE features (Kingma and Welling, 2014) and CLIP text features as latent features. Similarly, the Brain-diffuser method (Ozcelik and VanRullen, 2023) utilizes the component of another type of diffusion model (Xu et al., 2022), CLIP text features, and CLIP vision features as well as VDVAE features (Child, 2021) as latent features. Both methods first generate initial images from translated VAE/VDVAE features. These initial images are then passed through the image-to-image pipeline of the diffusion model conditioned on the translated CLIP features, producing the final reconstructed images. They validated the reconstruction performance using the NSD dataset, preparing training and test data based on the data split provided by the NSD study. Thanks to the authors of these studies who made efforts to make their datasets and scripts publicly available, we were able to conduct our replication analysis effectively. We compared the reconstructed results of these two text-guided reconstruction methods with those from a previous image reconstruction method, iCNN (Shen et al., 2019b). For more information on datasets and reconstruction methods, see Material and Methods (“Datasets” or “Reconstruction methods”) or the original studies (Allen et al., 2022; Shen et al., 2019b; Takagi and Nishimoto, 2023b; Ozcelik and VanRullen, 2023).

#### 2.1.1 Observations: Failed replication and convincing reconstruction from random data

We first confirmed the reproduction of the findings of the text-guided reconstruction methods, particularly those of the Brain-diffuser study (Ozcelik and VanRullen, 2023) when applied to the NSD dataset (Figure 2a). The reconstructed images generated by the Brain-diffuser method effectively captured most of the layout and semantics of the test images. Although the reconstructed images produced by the StableDiffusionReconstruction method (Takagi and Nishimoto, 2023b) showed slightly degraded performance compared to the original paper, they still successfully captured the semantics of the test images. Notably, the iCNN method (Shen et al., 2019b) also performed well on the NSD dataset, with reconstructed images capturing the dominant structures of the objects within the images, consistent with the findings reported in the original study.

To further investigate the generalizability of the text-guided reconstruction methods, we attempted to replicate their performance using a different dataset, Deeprecon, which was originally collected for the study by Shen et al. (2019b). The Deeprecon dataset was specifically designed to avoid overlap between training and test sets, making it an ideal benchmark for evaluating the zero-shot prediction capabilities of reconstruction methods. However, the original Deeprecon dataset lacked the text annotations required by the text-guided reconstruction methods. To facilitate a fair comparison, we collected five text annotations for each training stimulus in the Deeprecon dataset through crowd-sourcing and used them to generate CLIP text features.

Despite the inclusion of these text annotations, the text-guided reconstruction methods failed to achieve the same level of performance on the Deeprecon dataset as they did on the NSD dataset. The reconstructed images produced by the text-guided methods exhibited photo-like appearances but suffered from largely degraded quality compared to their performance on the NSD dataset (Figure 2b). Notably, the text-guided reconstruction methods generated photo-like reconstructions even for simple geometric shapes present in the Deeprecon dataset, which deviated significantly from the original stimuli. In contrast, the iCNN method (Shen et al., 2019a) consistently provided faithful reconstructions for both the NSD and Deeprecon datasets, despite its simplicity compared to the text-guided methods.

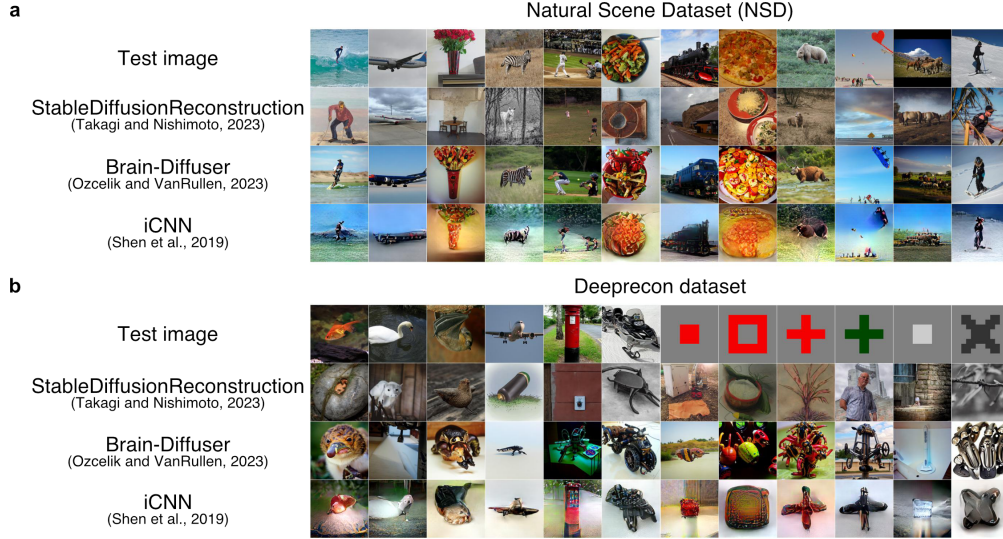


Figure 2: Image reconstruction results. (a) Reconstruction results for the NSD. The first row shows the original test images, followed by reconstructions using StableDiffusionReconstruction, Brain-Diffuser, and iCNN methods. (b) Reconstruction results for the Deeprecon dataset. The format is the same as in (a).

Upon further investigation, we noted a questionable post-hoc image selection procedure. In the StableDiffusionReconstruction study (Takagi and Nishimoto, 2023b), they presented the reconstruction results by the following procedure: “We generated five images for each test image and selected the generated images with highest PSM” (PSM means perceptual similarity metrics), as illustrated in Figure 3a. This selection might lead readers or peer reviewers, particularly those not specialized in the brain decoding field, to overestimate the effectiveness of the methods and potentially lead to a distorted understanding of the actual reconstruction performance. Note that Brain-diffuser study (Ozcelik and VanRullen, 2023) did not execute such procedures and in their following report (Takagi and Nishimoto, 2023a), they updated the image presentation procedure more fairly as: “we generated five images with different stochastic noise and selected three images randomly.”

To examine the impact of this post-hoc selection procedure, we conducted an experiment using random brain data (Figure 3b). Instead of feeding the test brain data into pretrained translators, we shuffled the activities within each voxel of the NSD test set independently to create random brain data. Surprisingly, when the random brain data were input into the VAE feature translator, which contributes to producing initial images, plausible images were obtained by

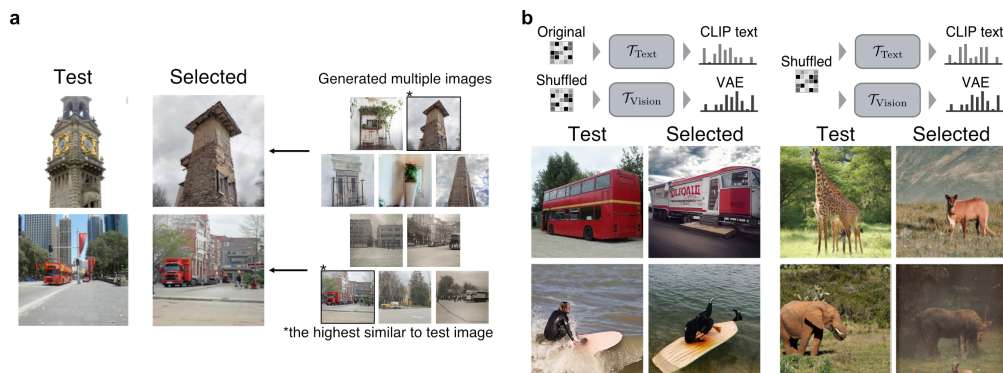


Figure 3: Questionable post-hoc selection. (a) Procedure in the StableDiffusionReconstruction method. Five images were generated, and the one that most closely resembled the test images was selected. (b) Reconstruction using shuffled brain activity. The left panels show the images generated from the VAE features given shuffled brain activity and CLIP text features given original brain activity. The right panels show the images generated from the VAE and CLIP text features given shuffled brain activity.

generating five images and selecting the best one. Even more strikingly, when the random brain data were input into both VAE and CLIP text feature translators, we still obtained convincing results by simply generating images five times and conducting the aforementioned selection. These observations are inexplicable since the artificially created brain data should completely lack any information related to the original visual stimuli.

These observations raise perplexing questions about the performance and generalizability of recent text-guided reconstruction methods. The significant deterioration in performance when simply changing the dataset from NSD to Deeprecon highlights the need for a deeper understanding of the factors contributing to the success of these methods on the NSD dataset. Moreover, the ability to obtain plausible reconstructions from random brain data by merely generating multiple images and selecting the best ones suggests that there may be fundamental issues with both the evaluation dataset and the components of the reconstruction methods themselves. In the following sections, we will conduct a thorough investigation into the potential problems associated with the NSD dataset and each component of the text-guided reconstruction pipeline.

### 2.1.2 Lack of diversity in the stimulus set

First, we examined the characteristics and limitations of the NSD dataset itself. To characterize the diversity of stimuli in the datasets and their latent representations, we focused on the CLIP features, which are used as latent features in recent reconstruction methods. We employed uniform manifold approximation and projection (UMAP) (McInnes et al., 2018) to visualize the CLIP text features of the NSD stimuli (see Materials and Methods “UMAP visualization”). The visualization revealed approximately 40 distinct clusters, with considerable overlap between the training and test sets (Figure 4a). Interestingly, we were able to describe the stimulus images in each cluster using a single semantic word, such as airplane, giraffe, or tennis. Despite the NSD containing around 30,000 brain samples per subject, the diversity of the presented stimuli was quite limited to just around 40 semantic concepts. In contrast, the Deeprecon dataset, which was specifically designed to differentiate object categories between training and test data, exhibited less overlap between the two sets (Supplementary Figure S1).

To further investigate the similarity between the training and test stimuli, we conducted an analysis using a state-of-the-art perceptual similarity metric called DreamSim (Fu et al., 2023) (Figure 4b). For each test image in the NSD, we used DreamSim to identify the most similar training images based on their perceptual similarity scores. We observed that the training images extracted using DreamSim were highly similar to the test images in the NSD, not only in terms of semantic concepts but also in terms of overall layout and visual composition. This finding suggests that the NSD test images are heavily biased towards the distribution of the training data, with a significant overlap in the visual and semantic features present in both sets. Such a strong bias raises concerns about the true reconstruction performance of methods evaluated on this dataset, as the impressive results may be largely attributable to the methods’ ability to memorize and reproduce the characteristics of the training data rather than generalizing to novel stimuli.

In contrast, when we applied the same DreamSim-based analysis to the Deeprecon dataset, we found that the extracted training images were substantially different from the test images. This observation indicates a clearer separation between the training and test distributions in the Deeprecon dataset, with the test images containing novel visual and semantic features that are not well-represented in the training set. The distinct differences between the NSD and Deeprecon datasets in terms of stimulus similarity highlight the importance of carefully designing evaluation benchmarks that can effectively assess the generalization capabilities of visual image reconstruction methods.

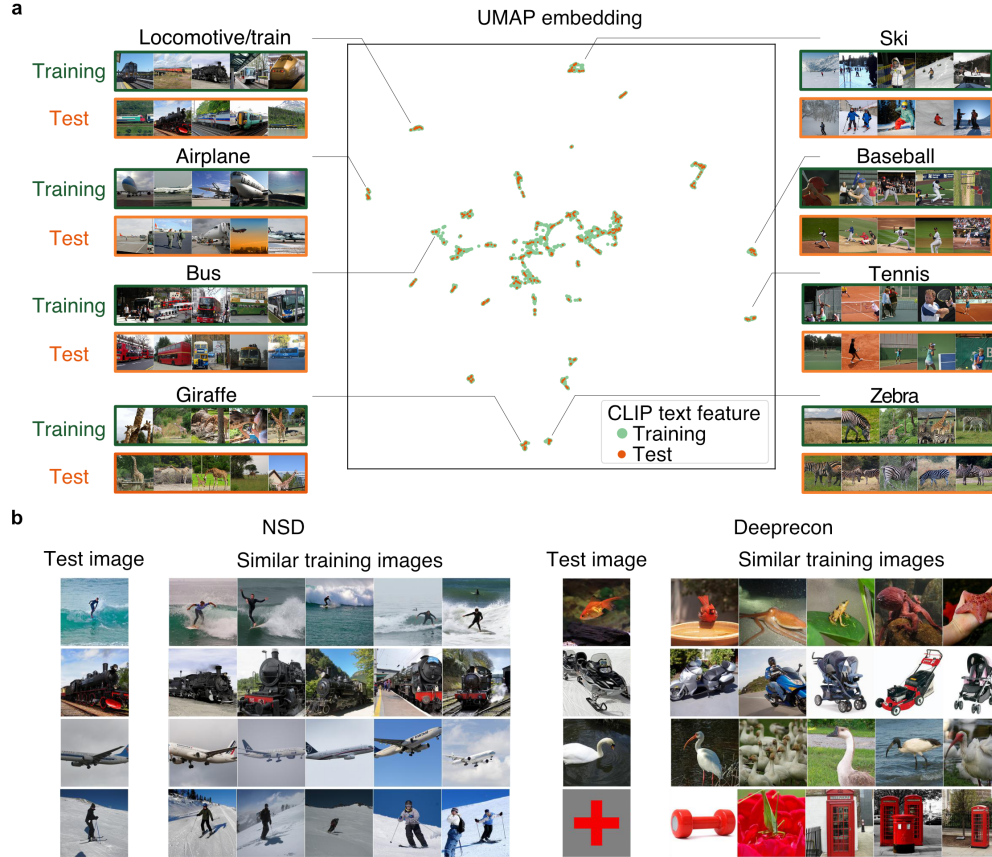


Figure 4: Dataset analysis. (a) UMAP visualization of CLIP text features in NSD. The center figure shows the scatter plot of the UMAP embedding of CLIP text features in NSD. Green points represent training samples, while orange points represent test samples. The surrounding images show the images in cluster. The presented images in each cluster were randomly selected. (b) Similarity between training and test images using the DreamSim metric. The left side shows results for the NSD, and the right side shows results for the Deeprecon dataset. The top 5 training images with highest similarity to each test image were selected.



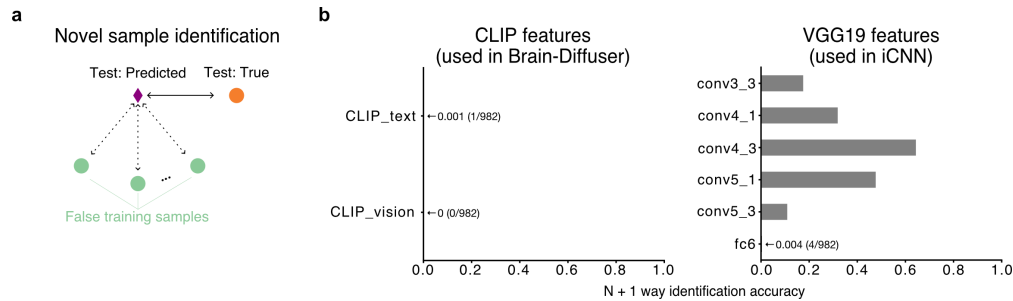


Figure 5: Zero-shot sample identification. (a) Schematic diagram of novel sample identification: calculating the similarity between predicted features and test features or each of the training features, and counting how many predicted features were more similar to the true features than other candidate training features. (b) Results for NSD. The left side shows the identification accuracies evaluated on the CLIP features, which were used in the Brain-diffuser methods. The right side shows the accuracies evaluated on several VGG19 features used in the iCNN method.

### 2.1.3 Failed zero-shot prediction in the feature space

Given the significant semantic and structural similarities between the NSD test images and the training images, it is crucial to assess whether the predictions made from brain activity truly demonstrate generalization beyond the training set (i.e., zero-shot prediction). To evaluate the zero-shot prediction capability of the translators used in the reconstruction methods, we conducted an  $N + 1$  way identification analysis, where  $N$  represents all of the training samples and 1 refers to the test sample (Figure 5a). We calculated the percentage of translated features that successfully identified the corresponding test sample in the NSD dataset.

The performance of the CLIP features was nearly 0% (Figure 5b). This extremely low performance suggests that the CLIP feature translator fails to achieve zero-shot prediction, even within the distribution covered by the training set. In other words, the CLIP features translated from brain activity are unable to accurately identify novel test samples, indicating a lack of generalizability beyond the training data. In contrast, the VGG19 features (Simonyan and Zisserman, 2015) employed in the iCNN method demonstrated moderate identification performance at the latent features on the intermediate layers. This finding suggests that the VGG19 features possess a certain degree of generalizability, enabling them to identify test samples that were not encountered during training.

Furthermore, we investigated whether the CLIP feature translator enables the prediction of novel semantic concepts not in the training. We redesigned the dataset split to ensure no semantic concepts were shared between them as in the previous zero-shot prediction study (Mitchell et al., 2008; Brouwer and Heeger, 2009). We first applied  $k$ -means clustering to the UMAP embedding space of the NSD’s CLIP text features (Supplementary Figure S2a). We set the number of clusters as 40 based on visual inspection of the UMAP results. Based on these clustering results, we performed a hold-out analysis: when predicting samples within a cluster (e.g., the ski cluster), we excluded samples from that cluster in the training set (Figure 6a; hold-out split condition). As a control, we also prepared a naive data-split condition where the training sample size is the same as in the hold-out split condition but allows overlapping semantic concepts. When we visualized the properties of predicted features in hold-out analysis by transforming the predicted features into the previous UMAP embedding space (Figure 4a), we observed that the predicted features tend to diverge largely from their original clusters and move into other clusters (Figure 6b).

To quantitatively assess the performance of the feature translator, we employed two metrics: cluster identification accuracy and pairwise sample identification accuracy. Cluster identification accuracy focuses on evaluating the translator’s ability to generate features that correctly identify the semantic cluster to which a test sample belongs (Figure 6c; left). In this analysis, we compare the predicted features of each test sample to the average features of the training samples within each semantic cluster. The accuracy is then calculated as the percentage of predicted features that successfully identify the original semantic cluster of their corresponding test samples in the feature space. Pairwise sample identification accuracy is a commonly used metric in the evaluation of feature prediction and reconstruction performance (Beliy et al., 2019; Shen et al., 2019b,a; Mozafari et al., 2020; Qiao et al., 2020; Ren et al., 2021; Gaziv et al., 2022; Takagi and Nishimoto, 2023b; Ozcelik and VanRullen, 2023; Ferrante et al., 2023; Scotti et al., 2023; Denk et al., 2023; Koide-Majima et al., 2024). This analysis assesses the translator’s ability to generate features that are more similar to the actual test features than to the features of other samples in the test set (Figure 6c; right). For each test sample, we compare its predicted features with two sets of features: the actual test features and the features of another randomly selected sample from the test set. The accuracy is then calculated as the average winning rate of the predicted

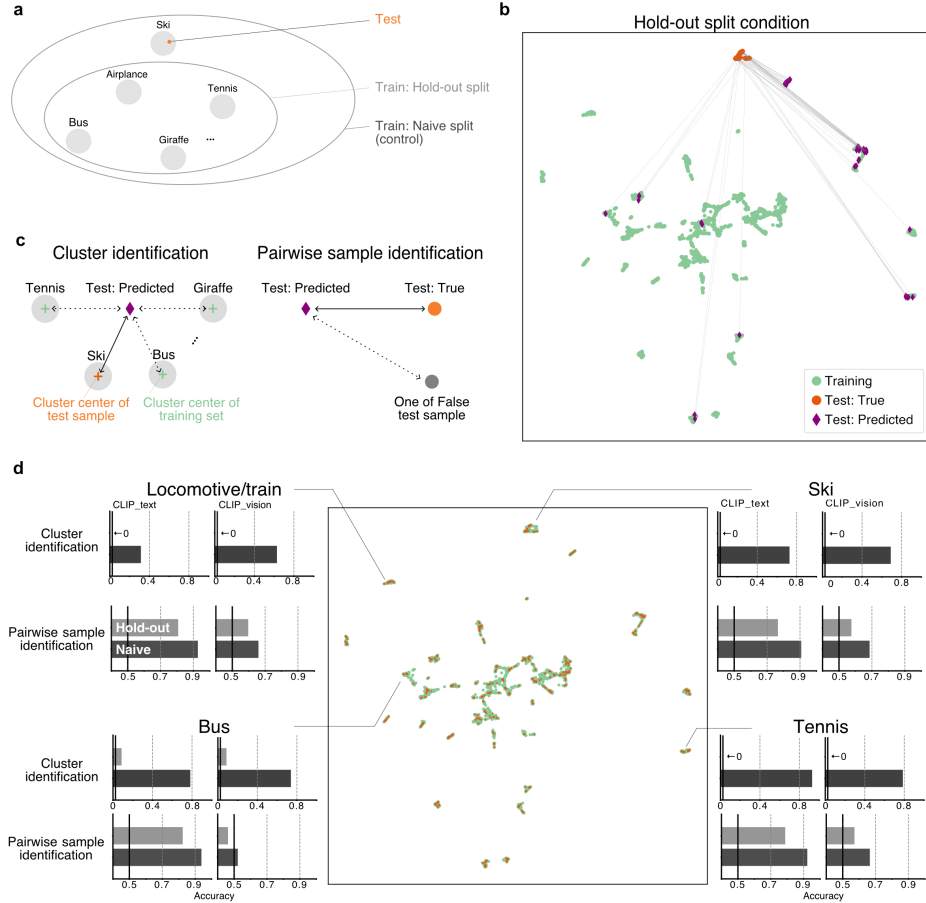


Figure 6: Zero-shot cluster identification. (a) Conceptual diagram of hold-out analysis. For predictions of test samples in a cluster, training samples belonging to the cluster were excluded. The naive split condition serves as a control, using the same number of training samples as in the hold-out split condition but allowing semantic concepts to overlap between training and test sets. (b) Representative example of feature translation under the hold-out split condition. The green and orange points represent training and test samples, respectively. The purple diamonds represent the translated (predicted) latent features. The gray lines represent the transition from the test sample to the corresponding predicted feature. (c) Two types of evaluation of predicted latent features. The left side shows the cluster identification accuracy, which compares predicted features to the average features of training samples within each cluster. The right side shows the pairwise sample identification accuracy, comparing predicted features with the test sample feature or with features of other test samples. (d) Feature prediction results. The four surrounding panels show the semantic clusters observed in the UMAP. In each panel, the upper graphs show the cluster identification performances for CLIP text and CLIP vision features. The expected chance level is  $1/40$ . The lower graphs show the pairwise sample identification performances for CLIP text and CLIP vision features. The expected chance level is  $1/2$ .

features against all other test samples, indicating the proportion of cases where the predicted features are more similar to the actual test features than to the features of other samples.

Figure 6d presents a comparison of the identification performance of the feature translator in each semantic cluster between the hold-out and naive split conditions, as measured by two evaluation metrics: cluster identification accuracy and pairwise sample identification accuracy. The cluster identification accuracy in the hold-out split condition exhibited a substantial drop compared to the naive split condition across all semantic clusters. Notably, the cluster identification accuracy was frequently found to be 0% in the hold-out split condition, exposing a severe limitation of the translator in novel semantic concepts that were absent from the training set (see also Supplementary Figure S2b). This finding strongly suggests that the CLIP feature translator functions primarily as a “classifier,” heavily relying on the semantic features learned during the training phase.

Intriguingly, despite the feature translator’s complete failure to identify semantic concepts in the hold-out split condition, the pairwise sample identification accuracy often surpassed the chance level across the semantic clusters (Figure 6d). The insensitivity of the pairwise sample identification accuracy to the translator’s inability to capture semantic concepts can be attributed to its emphasis on comparing the relative similarity between the predicted features and the actual test features, without taking into account the broader categorical context. This can lead to an inflated pairwise sample identification accuracy, potentially misrepresenting the true reconstruction performance and the translator’s ability to generalize to novel clusters. This observation raises concerns about the adequacy of using identification accuracy as the sole metric for evaluating reconstruction performance, a practice that has been widely adopted in many studies (Beliy et al., 2019; Shen et al., 2019a,b; Mozafari et al., 2020; Qiao et al., 2020; Ren et al., 2021; Gaziv et al., 2022; Takagi and Nishimoto, 2023b; Ozcelik and VanRullen, 2023; Ferrante et al., 2023; Scotti et al., 2023; Denk et al., 2023; Koide-Majima et al., 2024).

#### 2.1.4 Failed recovery of a stimulus from its latent features

Finally, we conducted a rigorous evaluation of the generator component, which typically consists of diffusion models in generative AI-based reconstruction methods. To ensure that a visual image reconstruction method has the potential to faithfully reproduce an individual’s perceived visual experiences, it is crucial that the method can recover the original images with a high degree of perceptual similarity when the neural translation from brain activity to latent features is perfect. However, it has been unclear whether generative AI-based reconstruction methods meet this fundamental requirement. To address this question, we performed a recovery check analysis by reconstructing images using the true latent features of target images. Instead of using latent features transformed from brain activity, we directly input the latent features derived from the target images into the generator. While generative AI-based reconstruction methods generated images that were semantically similar to the target, the resulting images were not perceptually similar to the original (Figure 7a). In contrast, iCNN method yielded results that closely resembled the actual target images, demonstrating their superior ability to capture and replicate the original visual content.

To further investigate the recovery performance, we conducted a recovery check on each latent feature of the Brain-diffuser method (Figure 7b). Interestingly, reconstructions from VDVAE features, which are used for generating initial images in the Brain-diffuser, exhibited a high degree of similarity to the target images. However, the images generated by CLIP features through the diffusion models showed significant deviations from the original targets. These findings suggest that text-guided reconstruction methods may not be well-suited for visual image reconstruction tasks, as they fail

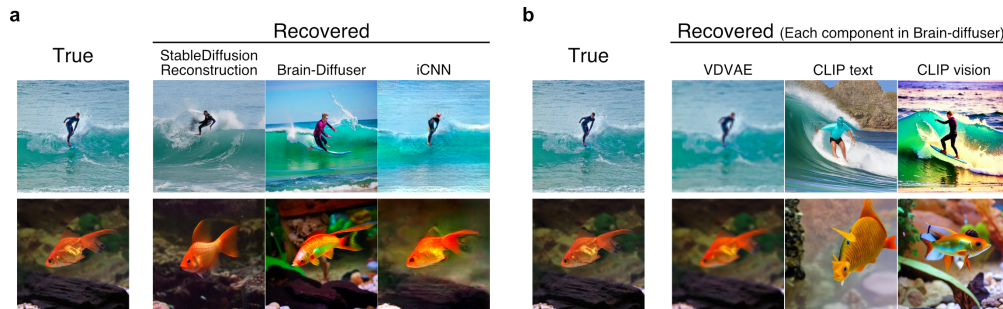


Figure 7: Recovery check. (a) Reconstruction from the true latent features. The left column shows the true images, followed by each method’s recovery results. (b) Reconstruction using each component of the Brain-diffuser method. The left column shows the true images, followed by the recovery results of each component of the Brain-diffuser method.



to faithfully recover the original visual images. Instead, they tend to create images based on their latent features, such as CLIP features, which can lead to a phenomenon known as “hallucination” in the field of generative AIs. Hallucination refers to an output that appears plausible but is actually incorrect or misleading, raising concerns about the reliability and accuracy of the model (Rawte et al., 2023). These methods seem to prioritize generating semantically similar images rather than faithfully reconstructing the visual content perceived by the individual.

These findings may provide an explanation for why the text-guided reconstruction methods performed well only on the NSD dataset. The results of the case study demonstrated that the text-guided reconstruction methods struggle to reconstruct (Figure 2) or identify (Figure 6) test samples that lie beyond the distribution of the training set. Such limitations suggest that these methods lack true generalization capabilities and are unable to accurately reconstruct novel visual experiences that differ significantly from the examples they were trained on. Moreover, even when the test samples belonged to the same distribution as the training set, the translators of the text-guided reconstruction methods had difficulty correctly identifying those test samples (Figure 5). This observation indicates that the translators may not have learned a sufficiently robust and generalizable mapping between brain activity patterns and the corresponding latent features, further limiting their ability to faithfully reconstruct the perceived visual experiences.

The case study revealed that the NSD test stimuli are highly similar to the training set (Figure 4), with a significant overlap in their visual and semantic features. Given this similarity, the impressive reconstruction results achieved by the recent text-guided reconstruction methods on the NSD dataset should not be interpreted as evidence of zero-shot reconstruction capabilities. Instead, a more plausible interpretation is that these methods primarily function as a combination of “classification” and “hallucination.”

In this context, the translator component of the text-guided reconstruction methods functions primarily as a classifier, predicting categorical information present in the training data rather than capturing the fine-grained details of the visual experience. This limitation may explain why convincing reconstructions can be obtained even from random brain data through post-hoc selection. Due to the limited variety in the outputs generated by the reconstruction models, repeated trials can eventually produce images that are semantically and visually similar to the target stimulus. The apparent plausibility and semantic consistency of these generated images can be attributed to the capabilities of the diffusion model, which learns to generate realistic-looking images based on the semantic information. While these images may seem convincing at first glance, they do not accurately reflect the specific visual experience of the individual. This phenomenon of hallucination raises serious concerns about the reliability and validity of the text-guided reconstruction methods when evaluated on the NSD dataset.

## 2.2 Formal analysis and simulation

In the above case study, we have identified several issues with these text-guided reconstruction methods and the dataset, especially the cluster structure of CLIP latent features, the lack of diversity in NSD, and the misspecification of the latent representation for image reconstruction, which results in the inability of diffusion models to faithfully recover the original images from their latent features. However, it is crucial to recognize that the findings of the case study are not merely specific to CLIP, NSD, or diffusion models. Instead, these issues likely reflect more fundamental problems that can arise in the development and evaluation of brain decoding and visual image reconstruction methods. Thus in this section, we extend the problems identified in the case study into formal analyses and simulations in generalized settings, aiming to provide a more comprehensive understanding of the factors that contribute to the limitations of current reconstruction methods and explore strategies for mitigating these issues.

### 2.2.1 Output dimension collapse

First, we revisit the properties of the translator and highlight the issues that arise when the prediction targets have insufficient diversity. Let us consider the general situation of predicting a feature  $\mathbf{y} \in \mathbb{R}^D$  from a brain activity pattern  $\mathbf{x} \in \mathbb{R}^D$  using a linear regression model. For the training set, we consider brain activity matrix  $X_{\text{tr}} \in \mathbb{R}^{N \times D}$  and feature value matrix  $Y_{\text{tr}} \in \mathbb{R}^{N \times D}$ , where  $X_{\text{tr}}$  consists of  $N$  samples of  $D$ -dimensional brain activity vectors  $\mathbf{x}$  and  $Y_{\text{tr}}$  consists of  $N$  feature value vectors  $\mathbf{y}$ . We then train the linear (ridge) regression model using this training data. Given a regularization parameter  $\lambda$ , the weight of ridge regression model is analytically derived as  $W = (X_{\text{tr}}^\top X_{\text{tr}} + \lambda I)^{-1} X_{\text{tr}}^\top Y_{\text{tr}}$ , where  $I$  is the  $D \times D$  identity matrix. The predicted feature value  $\hat{\mathbf{y}}_{\text{te}}$  for the test brain activity data  $\mathbf{x}_{\text{te}}$  can be represented as:

$$\hat{\mathbf{y}}_{\text{te}} = W^\top \mathbf{x}_{\text{te}} \quad (1)$$

$$= Y_{\text{tr}}^\top X_{\text{tr}} (X_{\text{tr}}^\top X_{\text{tr}} + \lambda I)^{-1} \mathbf{x}_{\text{te}} \quad (2)$$

$$= Y_{\text{tr}}^\top \mathbf{m} = \sum_i^N m_i \mathbf{y}_{\text{tr}}^{(i)}, \quad (3)$$

where  $\mathbf{m} = X_{\text{tr}}(X_{\text{tr}}^\top X_{\text{tr}} + \lambda I)^{-1} \mathbf{x}_{\text{te}} \in \mathbb{R}^{N \times 1}$  and  $\mathbf{y}_{\text{tr}}^{(i)}$  is the  $i$ th training feature vector. This transformation indicates that the predicted value is always represented as a linear combination of the features in the training set. This property is not limited to ridge regression but is generally applicable to ordinary ridgeless linear regression and related linear models.

Next, we consider a scenario where the diversity of the target features is small. This situation can arise when the feature space exhibits a clustered structure and the training data lacks sufficient diversity, as observed in the case study with the CLIP text features and the NSD dataset. When the training feature values have limited diversity, the predicted values from brain activity, which are represented as linear combinations of these features, also become constrained. Consequently, the prediction from brain data to features effectively becomes a projection onto a low-dimensional subspace formed by the training data.

To illustrate this phenomenon, we conducted a simple simulation to examine the distribution of predicted values from a linear regression model trained on clustered features (Figure 8). We generated clustered features by sampling from a Gaussian mixture distributions in a high-dimensional space. The corresponding brain activity data was generated from a multivariate Gaussian distribution. We then trained a linear regression model to predict the clustered feature values from the randomly generated brain data.

The simulation results clearly demonstrate the impact of clustered features on the predicted values. The trained model projects arbitrary brain data onto the subspace defined by the training features, resulting in predicted values that are confined to the vicinity of the training clusters. This observation highlights the limitation of training linear regression models with clustered features: the trained model’s predictions are inherently constrained by the diversity and structure of the training data.

This phenomenon, which we refer to as “output dimension collapse,” has important implications for the generalization capability of linear regression models in the context of brain decoding and visual image reconstruction. When the training data lacks diversity and forms distinct clusters in the feature space, the translator overly adapts to the subspace formed by the training data, regardless of the potential of the latent feature space. Consequently, the translator’s outputs become similar to patterns in the training set, irrespective of the inputs, severely limiting the model’s ability to predict novel or out-of-distribution samples. Note that output dimension collapse is not inherently caused by the limitations of linear regression models but rather stems from a lack of diversity in the outputs of the training data. This phenomenon can occur regardless of the type of regression model employed, including nonlinear models. In fact, nonlinear models may be even more susceptible to output dimension collapse, as the increased flexibility and complexity of these models can potentially exacerbate the issue.

Output dimension collapse may explain why plausible reconstructions were obtained even from random brain data by merely generating images several times in the case study. The NSD’s lack of semantic diversity causes the translator to

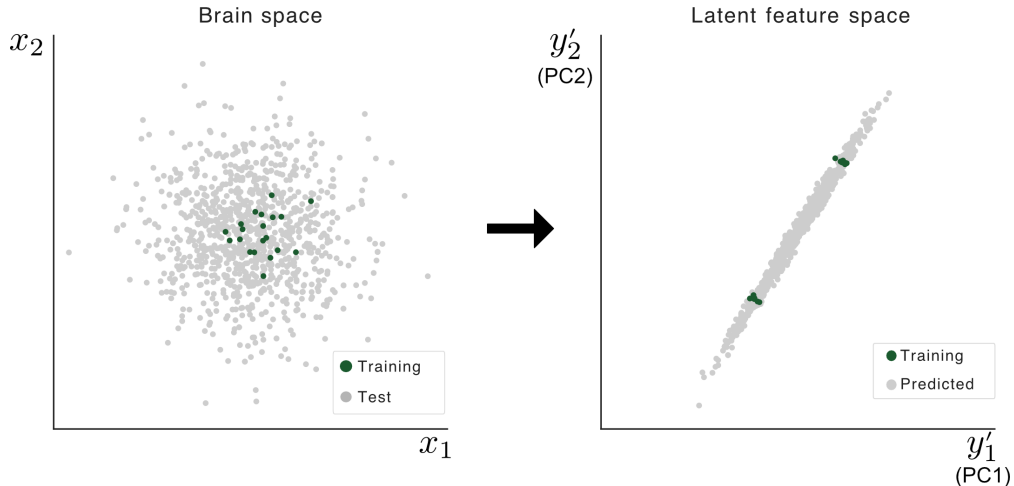


Figure 8: Output dimension collapse. The left panel shows the data distribution of source brain activity in the first two dimensions of high-dimensional space. The right panel shows the distribution of target latent features in the first two principal component (PC) dimensions. If the target features form a cluster structure in the high-dimensional space (left panel green points), the predictions (gray colors) fall into a subspace created by the training clusters, regardless of the input data (right panel).

adapt only to the feature patterns of the training set, restricting its outputs to the subspace formed by the training data. As a result, convincing images could be found even from random data through questionable post-hoc selection.

## 2.2.2 Simulation with clustered features: What makes prediction compositional

The case study revealed that the NSD exhibits limited diversity (Figure 4) and poses difficulties for zero-shot prediction (Figure 5 and 6). These observations suggest that the translator of CLIP features suffers from output dimension collapse due to the lack of semantic diversity in NSD. To explore potential strategies for mitigating output dimension collapse and achieving flexible predictions, we conducted simulation analyses using clustered data to assess generalization performance beyond the training set.

Our simulation involved teacher-student learning with Gaussian mixture models (see Materials and Methods: “Simulation with clustered data”). To imitate the feature translation situation from brain activity, we first generated feature data and assumed a scenario where observation noise affects the brain data. To simulate a situation where the dataset has cluster structures and to control diversity effectively, the training feature  $\mathbf{y} \in \mathbb{R}^D$  was generated from a  $D$ -dimensional mixture of Gaussians (Figure 9a). The brain activity data  $\mathbf{x} \in \mathbb{R}^D$  was generated from  $\mathbf{y}$  multiplied by teacher weight and adding observation noise.

We trained a ridge regression model on large training data samples and obtained the student weight. To simulate the situation where the trained model encounters clusters that are not available at the training phase, we generated two types of test samples, in-distribution and out-of-distribution. In-distribution test samples were generated using the same probability distribution as the training data, while out-of-distribution (OOD) samples were generated from a different distribution. For these two types of predicted features, we calculated the cluster identification accuracy (Figure 6c), using  $C + 1$  cluster centers, which included  $C$  centers from the training set and one additional center for the OOD test set.

We first examined zero-shot prediction performance as the number of clusters in the training data was increased while fixing the feature dimension  $D$  and the cluster variance ratio between each cluster constant (Figure 9b). While the cluster identification performance of in-distribution samples were perfect, that of OOD samples showed different patterns depending on the number of clusters in the training data. When the number of training clusters was low, cluster identification accuracy was 0%. This indicates that the behavior of the translator became more similar to a classifier, difficult to generalize beyond the training set, as observed in NSD cases (see also Figure 6d). On the other hand, as the number of clusters in the training data increased, it became possible to identify the novel clusters, achieving the same performance as in-distribution test samples. This observation indicates the importance of the diversity of the training dataset. We also emphasize that large numbers of training data do not necessarily address the problem. All of these results were obtained with a sufficiently large number of training data, and the number of training clusters was varied while keeping the number of training data fixed. Also, we observed qualitatively similar results in increasing the data diversity by controlling the cluster variance ratio (Supplementary Figure S3a).

Next, we investigate how diverse the training data needs to be to ensure sufficient generalization. There are two possible scenarios for diversifying training samples: either by densely sampling the entire space so that there are no remaining gaps or by uniformly sampling to the extent that it covers the entire dimension of the feature space (Figure 9c). The former scenario requires an exponentially larger number of samples relative to the dimension while the latter scenario only requires up to a linear order. We sought to reveal which of these two scenarios was more likely to be true by varying the dimensions of the feature space and identifying the number of clusters required for generalization (see also Supplementary Figure S3b). Here, we defined the number of clusters required for generalization as the point at which the prediction accuracy of OOD samples exceeds 50%. The relationship between the dimension of the feature space and the number of clusters necessary for generalization appears to be linear (Figure 9d). This finding suggests that achieving generalization does not necessarily require an exponentially large diversity that fills the entire feature space. Instead, it suffices to have a number of clusters that cover the effective dimensions within the feature space. Although obtaining a large amount of brain data is hard work, it is important for a dataset to contain sufficiently diverse stimuli covering the effective dimensions of the target feature space to achieve zero-shot prediction.

We also confirmed this phenomenon by a simple and transparent example ( $D = 2$ , Figure 9e). The training data covers sufficient axes in the feature space, enabling the prediction of locations not present in the training set. Based on this low dimensional intuition, we argue that successful zero-shot prediction requires that training data leads to representations that can serve as a basis spanning the feature space. Leveraging such bases effectively enables the model to predict novel samples by predicting each basis and combining them. This compositional representation, spanning the target feature space is crucial for zero-shot prediction (Schug et al., 2024) and reconstructing arbitrary visual images from limited brain data.

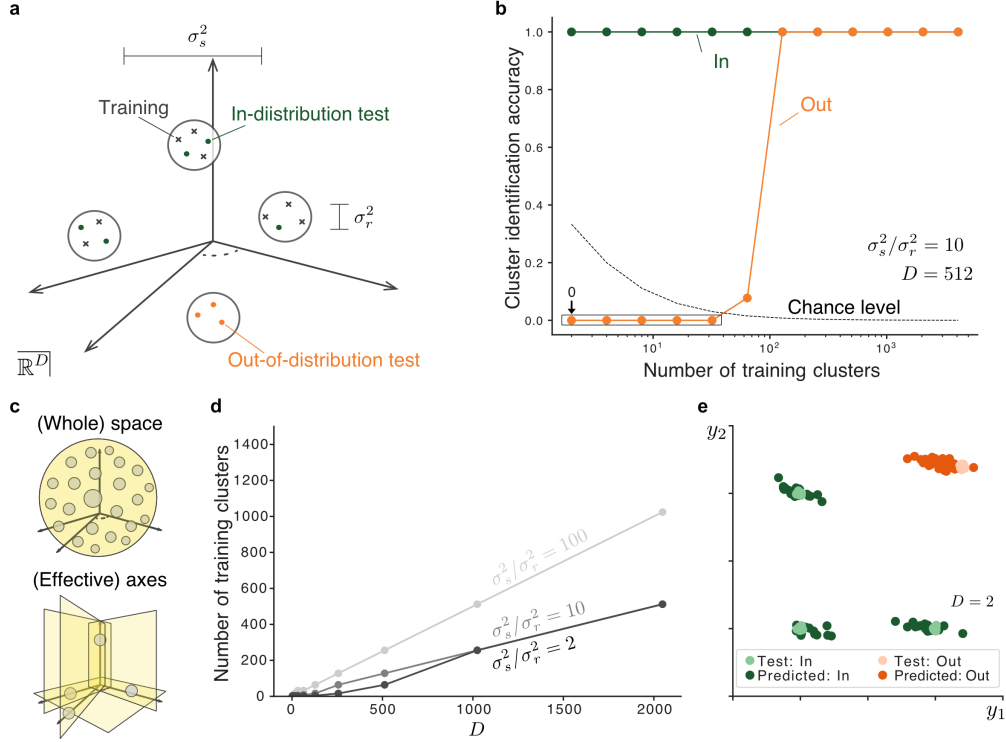


Figure 9: Simulation analysis of predicting features with cluster structure. (a) Illustration of target latent features setting. The latent features were generated from Gaussian mixture distributions.  $\sigma_r^2$  is a parameter of the sample variance of each cluster.  $\sigma_s^2$  controls the distance across clusters. In-distribution test samples are generated from the same clusters as in the training set. Out-of-distribution (OOD) test samples are generated from a novel cluster not included in the training set. (b) Cluster identification accuracy. The  $x$  axis represents the number of clusters used in the training and the  $y$  axis represents the cluster identification performance. Green line shows the results of In-distribution test samples and orange line shows those for OOD samples. Dashed curve indicates the chance level. (c) Illustration of a possible scenario where sufficient data diversity is needed to achieve generalizability. The upper illustration shows that the training data should cover the whole latent feature space, requiring an exponential order relative to the feature dimension. The lower one shows that the training data is covering only the effective axes of the latent feature space, leading to a linear order relative to the feature dimension. (d) Relation between latent feature dimension and sufficient number of clusters for generalization. The  $x$  axis represents the dimension of target latent features. The  $y$  axis represents the number of clusters that achieve above 0.5 cluster identification accuracy. Three lines indicate the results from different  $\sigma_s^2/\sigma_r^2$ . (e) Representative example of generalizability beyond the training set. Light green points indicate the in-distribution test samples while light orange points indicate OOD test samples. Green and orange points represent the predictions.

### 2.2.3 Preserved image information across hierarchical DNN layers

To enable the reconstruction for arbitrary visual images, compositional latent features that can be appropriately mapped into the image space are essential. Although it is often assumed that the hierarchical feature representations in DNNs, especially convolutional neural network (CNN), discard pixel-level information through their hierarchical processing with progressively expanding receptive fields, this is not necessarily the case.

For example, the latent features of auto-encoder models (Hinton and Salakhutdinov, 2006; Kingma and Welling, 2014; van den Oord et al., 2017) can represent images in a low-dimensional space while preserving their reversibility, which is reasonable considering that the output is trained to match the input. Furthermore, Mahendran and Vedaldi (2015) showed that input images can be reconstructed with reasonable accuracy even from relatively high-level layers of a DNN designed for an object recognition task. It has also been argued that large receptive field sizes do not necessarily impair neural coding capacity as long as the number and density of units remain constant (Zhang and Sejnowski, 1999; Majima et al., 2017). These results challenge the notion that higher-level layers in DNNs discard all pixel-level information and highlight the potential for utilizing intermediate representations in visual image reconstruction. To further illustrate this point, we performed a recovery check on each intermediate layer of the VGG19 network used in

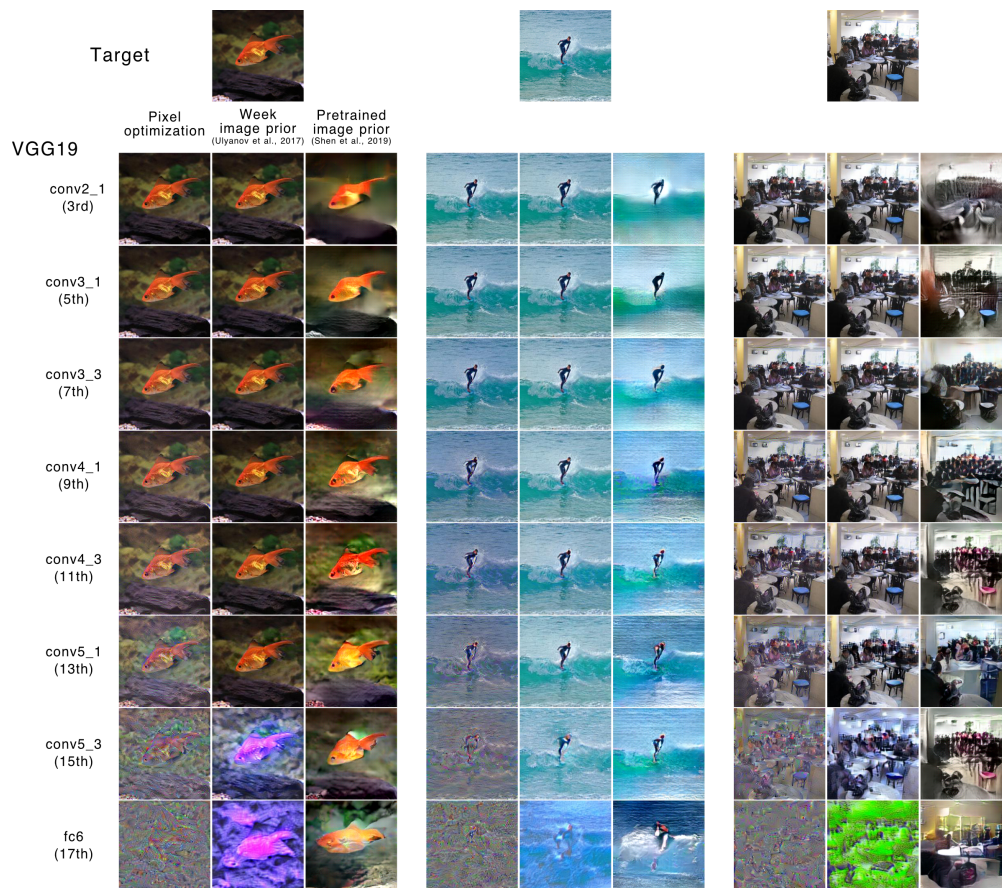


Figure 10: Recovery check: single layer used in iCNN method. For three images, the different optimization algorithm is applied to recover the visual input. The left one is pixel optimization, which directly optimizes the pixel values so that the loss between that generated image feature and target image features is minimized. The middle one is optimization with week image prior, which optimizes the parameters of image prior models and their latent features simultaneously (see Material and methods). The right one is optimization with pretrained image prior, which optimizes the latent features of the fixed image generator model so that the loss between the output image features and target image features is minimized.

the iCNN methods (Figure 10; see also Figure 7). Given the DNN features of a target image, we optimized input pixel values to make the image’s latent features similar to the targets (See Materials and Methods “Recovery check of a single layer by iCNN”). We observed that input images can be recovered with reasonable accuracy from relatively high-level layers (around the 11th layers, the 19th layers as a total). Furthermore, by introducing image generator networks to add constraints on image statistics, reasonable recovery can be achieved from even higher layers. By utilizing a weak image prior (Ulyanov et al., 2017), which contains only information about the structure of images without any prior information on natural images, input images can be recovered from the 13th layer. When using an image generator that has learned natural image information (Shen et al., 2019b; Dosovitskiy and Brox, 2016), input images can be recovered even from the 15th layer.

These findings underscore the significance of intermediate DNN representations that can effectively recover the input image in visual image reconstruction studies. Conversely, utilizing high-level image features or features from other modalities, such as text annotations, for which the corresponding images are challenging to recover, is not a rational choice for visual image reconstruction tasks. Although recent text-to-image models and decoded text features can easily generate images, the outputs should not be interpreted as reconstruction results. Instead, it is more reasonable to interpret them as visualizations of decoded semantic information.

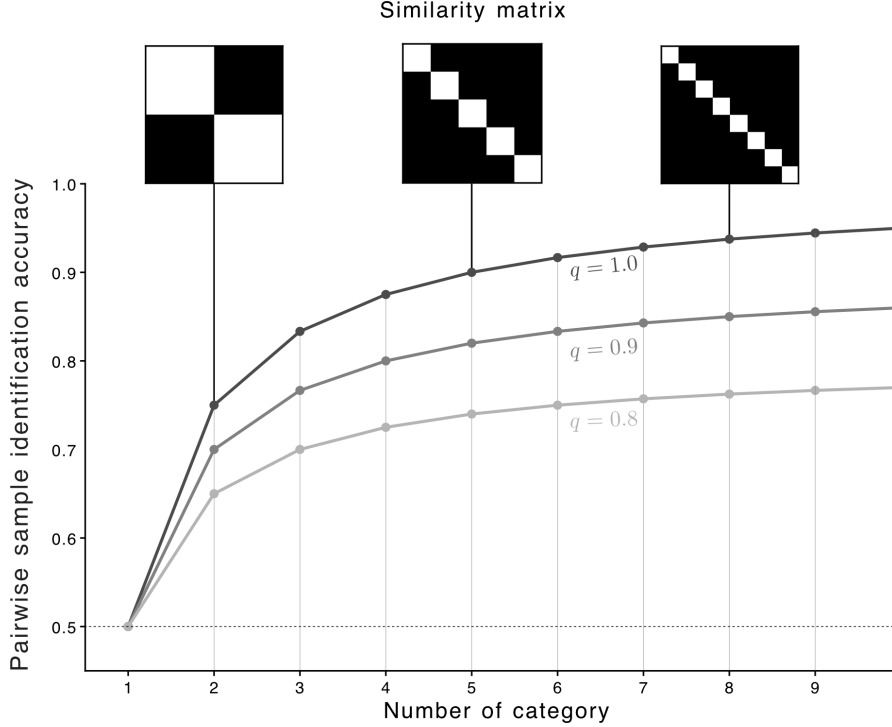


Figure 11: Pairwise sample identification with structured data. The  $x$  axis represents the number of categories in the test set. The  $y$  axis represents the pairwise sample identification accuracy. The lines show the different accuracy  $q$  in the situations where the candidate sample is from a different category than those in the test samples. The representative similarity matrices corresponding to these conditions are shown in the figure above.

#### 2.2.4 Caveat with evaluation by identification

Pairwise identification has been a standard metric for evaluating latent feature decoding (Horikawa and Kamitani, 2017) or reconstruction performance (Beliy et al., 2019; Shen et al., 2019a,b; Mozafari et al., 2020; Qiao et al., 2020; Ren et al., 2021; Gaziv et al., 2022; Takagi and Nishimoto, 2023b; Ozcelik and VanRullen, 2023; Ferrante et al., 2023; Scotti et al., 2023; Denk et al., 2023; Koide-Majima et al., 2024). However, our analysis revealed that even with difficulties in accurately identifying semantic clusters the test samples belong to, pairwise identification performance still surpassed chance levels (Figure 6d). Here we critically examine this metric and demonstrate that significant results can be easily obtained when the target or predicted features exhibit certain structures.

Pairwise identification is calculated as the accuracy with which the predicted features (reconstructed image or its features) can correctly identify the true ones, in pairs consisting of a true sample and one of the remaining samples in the test set. If the candidate feature belongs to the same category as the true feature, we can expect the identification to be difficult. Conversely, if the candidate feature belongs to a different category from the true feature, identification would become easier.

Here we assume the test set comprises  $k$  categories and all test samples are equally distributed across each category for simplicity. We model the situation mentioned above as the expected identification accuracy is set to chance level (i.e., 0.5) when a candidate belongs to the same category as the true feature. In contrast, the expected identification accuracy when a candidate belongs to a different category from the true feature is set to  $q$ , ranging between 0.5 to 1 to mimic the ease of identification across categories. Assuming the number of test samples is large enough, the pairwise identification becomes

$$\text{Acc} = \frac{1}{k} \cdot 0.5 + \left(1 - \frac{1}{k}\right) \cdot q \quad (4)$$

(See Materials and Methods “Expected identification accuracy in imprecise reconstructions” for the derivation). Figure 11 shows the line plots of expected values of pairwise identification accuracy as a function of the number of categories in the test set, while presenting the possible similarity structure of the test set. Even with failure to identify within categories completely and success only between two categories, pairwise identification accuracy can still reach a



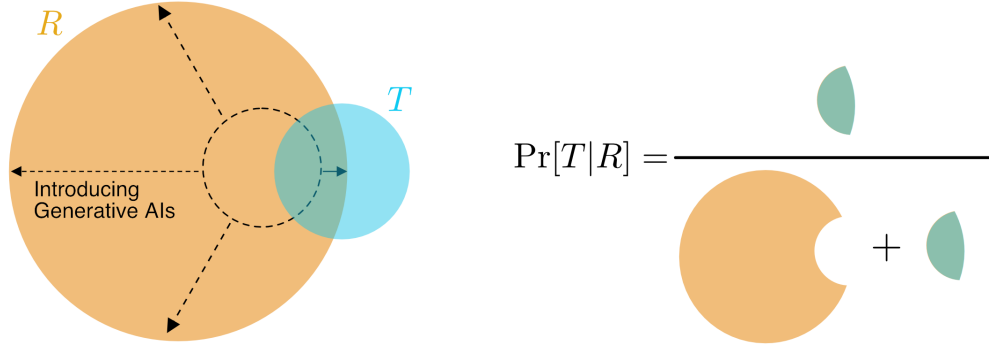


Figure 12: The dangerous interpretation of photo-like appearances as accurately reflecting the perceived visual image. The left Venn diagram represents the interpretation of photo-like reconstructions.  $T$  denotes the event where the generator’s output accurately reflects the visual image and  $R$  denotes the event where the generator’s output has a photo-like appearance. Introducing generative AIs (diffusion models) might increase the overlap between  $T$  and  $R$ ; however, it may also significantly increase the areas unrelated to  $T$ . The right equation represents the probability that the generator’s output accurately reflects the visual image given that the generator’s output has a photo-like appearance as inferred from the left Venn diagram.

high value up to 75%. This finding highlights a potential limitation of the pairwise identification metric, as judging reconstruction performance solely based on it can be misleading.

### 2.2.5 How are we fooled by hallucinations of generative AIs

Generative AIs have recently made remarkable progress, with models now capable of producing high-resolution and hyper-realistic images from text input (Ramesh et al., 2021) or generating text of a quality indistinguishable from human-written content (Brown et al., 2020). However, due to the complex internal structure of these models and the vast amounts of data they are trained on, we are often fooled by the outputs of generative AIs. For instance, when searching for an unfamiliar topic using a large language model (LLM) in our daily life, we may not realize that the model is creating false concepts. Someone may have mistaken generative AI show real-time response in the promotion, despite the fact that these promotions were edited (Coldewey, 2023). We might also believe that these models are unbiased or can represent all possible viewpoints, even though they inherently contain biases from their training data and developers (Messori and Crockett, 2024). As we have observed that the generative AI-based reconstruction methods exhibit photo-like appearances but poor generalizability (Figure 2), could similar issues be occurring in visual image reconstruction studies as well?

The goal of visual image reconstruction is to generate images from brain activity that precisely mirror visual experience. However, there appears to be a prevalent focus among the general public, reviewers, and even researchers on achieving outputs that are as photorealistic as possible, rather than emphasizing the accuracy of these reconstructions. This shift in focus raises questions about the extent to which these photorealistic reconstructions truly represent the actual visual experiences.

Traditionally, we have held two beliefs: 1) generating photo-like images from brain activity is challenging, and 2) if the reconstruction pipeline effectively captures the brain representation under natural image perception, the model’s output should also appear naturalistic or photo-like. Based on these beliefs, we tend to consider photo-like reconstructions as an indication of accurately reflecting the actual visual experience.

This heuristic can be formalized as follows:

$$\text{Assumption 1: } \Pr[R] \ll \Pr[\bar{R}] \approx 1, \quad (5)$$

$$\text{Assumption 2: } \Pr[R | T] \approx 1, \quad (6)$$

$$\text{Conclusion: } \Pr[T | R] \text{ is high}, \quad (7)$$

where  $T$  represents the event of the model’s output truthfully reflects the visual image and  $R$  represents the event of the model’s output has a realistic appearance.  $\bar{R}$  represents a complementary event of  $R$ .  $\Pr[T | R]$  is the probability that how likely we should conclude that the model’s output actually reflects the subject’s visual experience based solely on the fact that the output is photo-like. In fact, this heuristic is reasonable when the above two assumptions are true and  $\Pr[T]$  is not extremely low.

However, recent developments in generative AIs, such as diffusion models, have made it easy to produce convincing photo-like outputs, subverting the first assumption i.e.,  $\Pr[R] \gg \Pr[\bar{R}]$ . Consequently, it becomes invalid to infer that the visual images are accurately reflected in the generator outputs solely because they appear photo-like. Rather, as shown in Figure 12, the probability  $\Pr[T | R]$  may become smaller as the generative AIs produce more convincing outputs (see also Figure 7). This perspective emphasizes the need for careful evaluation of reconstruction performance, considering the possibility of hallucinations by generators. While pursuing photo-like reconstructions to improve reconstruction fidelity is undoubtedly important, it would be counterproductive to obsess over naturalistic appearance to the point of neglecting the original goal of reconstructing perceived visual images.

### 3 Discussion

In this study, we critically examined recent generative AI-based visual image reconstruction methods to assess their true capabilities and limitations. Our primary goals were to (1) investigate the performance of these methods on different datasets, (2) identify potential issues and pitfalls in their methodology and evaluation, and (3) provide insights and recommendations for future research in this field. We conducted a case study focusing on text-guided reconstruction methods and their validation on the Natural Scene Dataset (NSD). Our findings revealed several concerns, including the failure to replicate the reconstruction performance on a different dataset, the use of problematic post-hoc image selection procedures, the lack of diversity and limited number of clusters in the NSD stimulus set, the failure of zero-shot prediction by the translator component, and the inability to accurately recover original stimuli by the generator component. Formal analysis and simulations further demonstrated the phenomenon of output dimension collapse, the importance of compositional representations for achieving zero-shot prediction, and the potential pitfalls of relying solely on identification metrics to evaluate reconstruction performance. Moreover, we highlighted that photo-like appearance does not necessarily imply accurate reflection of the perceived visual images. Based on these findings, we argue that the reconstructions from the recent text-guided reconstruction methods are, in large part, the result of a combination of classification and hallucination. Our study emphasizes the need for more rigorous evaluation and careful interpretation of results in visual image reconstruction research, particularly when using generative AI-based methods.

While our study critically examined the limitations of recent text-guided, diffusion-based methods for visual image reconstruction, it is important to acknowledge that these approaches provide new and potentially promising directions for brain decoding research. Although we emphasized the importance of achieving zero-shot prediction, it is crucial to recognize that most brain decoding studies focus on classification tasks, which, while not zero-shot, have provided insights into neural representations (Kamitani and Tong, 2005; Haxby et al., 2001). Moreover, the visualization of semantic contents (e.g., the supplementary movies in Horikawa et al. (2013)), can have significant utility in visual communication, even if it does not constitute zero-shot prediction. It is also worth noting that the individual components of these text-guided, diffusion-based methods are already being utilized in various brain decoding applications. For instance, text latent features derived from deep neural networks and large language models (LLMs) have shown promise in analyzing semantic information from brain activity (Tang et al., 2023; Caucheteux et al., 2023; Zhou et al., 2024). Furthermore, diffusion models are not limited to text-to-image generation; they can be trained to generate images from visual latent features, as demonstrated by Cheng et al. (2023), enabling the successful reconstruction of subjective experiences. By leveraging these components and exploring their potential synergies, researchers can continue to push the boundaries of brain decoding and visual image reconstruction, while being mindful of the challenges and limitations highlighted in our study.

The recent trend of collecting and sharing large-scale visual neural datasets, such as those by Hebart et al. (2023) and Xu et al. (2024), is a welcome development in the field of neuroscience. These datasets provide valuable resources for researchers to investigate brain function and advance our understanding of visual processing. The NSD is a particularly notable example, as it was created with the goal of extensively sampling brain responses to a wide range of natural visual stimuli (Allen et al., 2022; Naselaris et al., 2021). The NSD has been widely utilized in various studies (Prince et al., 2022; Conwell et al., 2023; Gifford et al., 2023), demonstrating its value to the research community. While our results suggest that the semantic and visual diversity of the NSD stimuli may not be as high as initially thought, and there is substantial overlap between the training and test sets provided by the NSD authors, this does not diminish the overall importance and usefulness of the dataset. However, to fully leverage the NSD and other publicly available large-scale datasets for developing generalizable and zero-shot prediction models, it is crucial to carefully consider the data split between training and test sets. When aiming for generalizable predictions, such as in visual image reconstruction, researchers should verify whether there are significantly similar stimuli included in both the training and test sets. If necessary, redesigning the training and test split can ensure that the models are tested on their ability to predict novel stimuli. Moreover, recent advancements in functional alignment and inter-site neural code conversion methods (Haxby et al., 2011; Yamada et al., 2015; Wang et al., 2024) hold promise for combining datasets from different sources, enabling truly larger-scale data analysis in neuroscience. These techniques allow researchers to align brain activity



patterns across individuals and measurement sites even when stimuli are not shared across datasets. By leveraging these methods, researchers can pool data from various sources, increasing the sample size and diversity of the combined dataset, mitigating the limitations of individual datasets, and enhancing the development of generalizable and zero-shot prediction models.

Investigating neural responses to natural stimuli is a highly valuable approach to understand brain function and representation (Nastase et al., 2020; Hasson et al., 2020). As our brains have developed while being exposed to natural scenes, it is crucial to use natural stimuli especially in model training. However, we should not forget that we are also capable of perceiving non-natural stimuli like artificial images. We would like to emphasize that there are the potential pitfalls when relying too heavily on evaluations based solely on natural stimuli. With the increasing scale of neural data and the growing complexity of analysis pipelines, there is a risk that the learned mappings may produce unexpected shortcuts, just as we have demonstrated that the generative AI-based reconstruction methods exploited the semantic and visual overlap between training and test sets. Drawing inspiration from comparative and developmental psychology, where researchers often employ simple stimuli and tasks to measure cognitive abilities in infants for better experimental control and precise inferences (Kominsky et al., 2022; Messeri and Crockett, 2024), the evaluation of visual image reconstruction should not be limited to complex natural stimuli alone. While natural stimuli are essential for ensuring ecological validity and understanding how the brain processes real-world information, it is equally important to assess the performance in controllable and transparent manners.

We discussed output dimension collapse and related issues with clustered data found in natural image features. It is important to note that these issues can arise in various situations. Several studies have used brain data where the stimuli shared the category information between the training and test sets. Kavasidis et al. (2017) collected a dataset of EEG signals recorded during natural image perception. Their visual stimuli consisted of 2,000 images selected from 40 object categories in ImageNet (50 images per category) and the test set contains the same categories that are included in the training set. Denk et al. (2023) attempted to develop music reconstruction methods from fMRI activity patterns. Their music stimuli consisted of 540 music pieces selected from 10 music genres and the test set contains the same genres as the training set (Nakai et al., 2021). Orima et al. (2024) attempted to reconstruct perceived texture images from EEG signals. Their texture stimuli consisted of 191 images of 21 natural textures and they performed a reconstruction analysis with a leave-one-out manner. It should be carefully examined whether these studies may suffer from output dimension collapse, merely decoding category information from brain activity and generating stimuli based on this classified category information, similar to our interpretation of the text-guided reconstruction methods. Note that for other issues in the data from Kavasidis et al. (2017), see Li et al. (2018); Xu et al. (2024). Our inspection of the data from Nishimoto et al. (2011) revealed that many frames in the test movie stimuli were almost identical to those in the training set (Supplementary Figure S4). This is presumably because temporally adjacent video frames were split between the training and test stimuli. While our preliminary analysis of their motion energy features did not exhibit peculiar clustering (note also that their model was an encoding model where the output is brain activity), caution should be exercised if the dataset is used for models that extract other features of the videos.

One of the remaining challenges in visual image reconstruction is the development of metrics for evaluating the quality and accuracy of the reconstructed images. The first and most critical step in assessing reconstruction results is to confirm a qualitative similarity between the reconstructed images and the perceived images through visual inspection across a diverse range of test sets. Following this, quantitative metrics should be employed for a more objective, high-throughput evaluation. However, as our analysis has suggested, it can be misleading to evaluate reconstruction by heavily relying on identification performance based on the relative similarity among alternatives (Koide-Majima et al., 2024). Even in cases where the reconstructed images only capture superficial information, such as categories or overall brightness, identification metrics can still be high. While identification performance can provide a useful benchmark, it should not be the sole metric for evaluating reconstruction quality. It is crucial to develop more appropriate similarity metrics that can accurately measure the perceptual similarity between the reconstructed and original images. One promising approach is to leverage image quality assessment (IQA) techniques from the computer vision field (Fu et al., 2023; Ding et al., 2020). These techniques are designed to quantify the perceptual quality of images and can be adapted to the specific requirements of visual image reconstruction.

Visual image reconstruction methods have gained attention not only from neuroscientists but also from the general public and policymakers, sparking discussions about their potential applications and risks (UNESCO, 2023). These stakeholders often contemplate the possibilities of seamless information communication through the brain, such as in brain-machine interfaces (BMIs), or the dangers of unauthorized access to private information from brain activity. This interest may stem from the perception that brain activity data can be obtained easily and reliably in real-time. However, current technology and analysis methods fall short of these expectations. For instance, most reconstruction methods analyze previously acquired brain data offline. Additionally, the brain data used for reconstructing images are often averaged over multiple presentations of the test image, with only a few studies demonstrating single-trial reconstruction results (Miyawaki et al., 2008; Cheng et al., 2023). Further, It has been argued that subject cooperation

is essential for reliably training and testing decoding models (Tang et al., 2023). Public expectations are thus set too high, and it is challenging to meet these demands quickly. It is essential to explicitly state these limitations to avoid disappointment and prevent governments or companies from making misguided decisions. Key limitations include the lack of real-time analysis, reliance on averaged brain data, the necessity of subject cooperation, and the need for further model fine-tuning using the test brain dataset (Beliy et al., 2019; Chen et al., 2023a). It is crucial to avoid making overly optimistic claims about the ability to reconstruct arbitrary images, as the applicability can be highly dependent on specific training data and conditions.

## 4 Materials and Methods

### 4.1 Datasets

We utilized two datasets: the natural scene dataset (NSD) (Allen et al., 2022) and Deeprecon dataset (Shen et al., 2019b). Both datasets comprise visual stimuli and corresponding fMRI activity collected when subjects perceived the stimuli. In the NSD dataset, eight subjects were presented with MSCOCO images (Lin et al., 2014), yielding 30,000 brain activity samples per subject, which is three times the amount provided by the Deeprecon dataset. The Deeprecon dataset includes fMRI activity data from subjects presented with both ImageNet images (Deng et al., 2009) and artificial images. It contains roughly 8,000 brain samples per subject. Since this dataset is designed for evaluating reconstruction performance, the test data is carefully selected. The test natural images were selected from ImageNet, which were in categories different from those used in the training. The artificial images were only used as test data to check the generalizability performance of the proposed reconstruction methods. In both datasets, we adopted the train/test split used in previous studies and utilized data from the first subject (S1 in NSD, Subject 1 in Deeprecon). Text-guided reconstruction methods require text annotations of images.. For the NSD, text annotations accompanying the MSCOCO database were used. For the Deeprecon dataset, we collected captions for each experimental stimulus via crowd workers on Amazon Mechanical Turk, yielding five captions per image. The captions of training stimuli are publicly available at the GitHub repository.

### 4.2 Reconstruction methods

We utilized three image reconstruction methods: StableDiffusionReconstruction (Takagi and Nishimoto, 2023b), Brain-diffuser (Ozcelik and VanRullen, 2023) and iCNN (Shen et al., 2019b). Each method employs two common steps: first, translating brain activity patterns into latent features of the stimuli, and second, generating images from these latent features using an image generator (see also Figure 1). In the StableDiffusionReconstruction method, the latent features are the VAE (Kingma and Welling, 2014) features calculated from stimulus images and CLIP text features (Radford et al., 2021) from the image annotations. The generator is StableDiffusion (Rombach et al., 2022). They first generate low-resolution images from the translated VAE features, and those images are further fed into the StableDiffusion model with translated text features to generate images. The generated images are regarded as reconstructed images from brain activity. In the Brain-diffuser method, the latent features are the VDVAE (Child, 2021) and CLIP vision features from stimulus images and CLIP text features from the image annotations. The generator is Versatile diffusion (Xu et al., 2022). Similar to StableDiffusionReconstruction, low-resolution images are first generated from the translated VDVAE features, and these images are further used for the input of the versatile diffusion model with the translated vision and text features. The generated images are regarded as reconstructed images from brain activity. In the iCNN method, the latent features are the intermediate output of VGG19 (Simonyan and Zisserman, 2015) layer from stimulus images. As a generator, they used the pretrained image generator (Dosovitskiy and Brox, 2016) and they solved the optimization problem to minimize the discrepancy between the VGG19 features calculated from the generated images and the transformed VGG19 features. Well-optimized images are regarded as reconstructed images.

### 4.3 UMAP visualization

To investigate dataset diversity, we employed Uniform Manifold Approximation and Projection (UMAP), a non-linear dimensionality reduction technique (McInnes et al., 2018) to learn a projection from a latent features space to a lower dimension (UMAP embedding space). We used both the training and test CLIP text features for learning the UMAP projection. These features were combined and standardized beforehand. The UMAP hyperparameters follow the official UMAP guide for clustering usage with cosine distance as a distance metric. The learned UMAP was also used to project the features predicted from brain activity (Figure 4). After standardizing the predicted features using the same mean and standard deviation parameters used in UMAP projection learning, we projected the decoded features into the UMAP embedding space.

#### 4.4 Simulation with clustered data

We conducted a simulation analysis to examine the generalization performance beyond the training data (Figure 6). This analysis involves a teacher-student learning task using Gaussian mixture distributions. We generated both input and target pairs from teachers, then examined the prediction performance of regression models of students. To imitate the feature translation situation from brain activity, we first generated feature data and assumed a scenario where observation noise affects the brain data.

The training sample of latent feature data  $\mathbf{y} \in \mathbb{R}^D$  was generated from a  $D$ -dimensional space using Gaussian mixture distributions, formulated as:

$$p_{\text{tr}}(\mathbf{y}) = \frac{1}{C} \sum_{c=1}^C \mathcal{N}(\boldsymbol{\mu}_c^{\text{tr}}, \sigma_r^2 I), \quad \boldsymbol{\mu}_c^{\text{tr}} \sim \mathcal{N}(\mathbf{0}, \sigma_s^2), \quad (8)$$

where  $C$  is the number of clusters in the training set.  $\sigma_r^2$  is the scalar value representing the variance of the Gaussian distribution corresponding to each cluster.  $\sigma_s^2$  is the scalar value representing the variance of the distribution of cluster centers ( $\boldsymbol{\mu}_c^{\text{tr}}$ ). Brain activity data,  $\mathbf{x} \in \mathbb{R}^D$ , were generated using teacher weights  $\bar{\mathbf{A}} \in \mathbb{R}^{D \times D}$  and incorporating observation noise  $\boldsymbol{\xi}$  with  $\mathbf{x} = \bar{\mathbf{A}}^\top \mathbf{y} + \boldsymbol{\xi}$ , where  $\boldsymbol{\xi} \sim \mathcal{N}(\mathbf{0}, \sigma_n^2 I)$ .  $\sigma_n^2$  is the scalar value representing the variance of observation noise. Using  $N$  training samples, the ridge regression model was trained. With the hyperparameter  $\lambda$ , the weight of ridge regression model  $\mathbf{W}$  can be calculated analytically:

$$\mathbf{W} = (\mathbf{X}_{\text{tr}}^\top \mathbf{X}_{\text{tr}} + \lambda I)^{-1} \mathbf{X}_{\text{tr}}^\top \mathbf{Y}_{\text{tr}}. \quad (9)$$

For testing the model performance, we prepared two types of test samples, in-distribution test samples and out-of-distribution test samples. In-distribution test samples are generated using the same parameter as  $p_{\text{tr}}(\mathbf{y})$ . Out-of-distribution (OOD) test samples were generated in two steps. First,  $C_{\text{ood}}$  different cluster centers  $\boldsymbol{\mu}_c^{\text{ood}}$  were obtained by sampling from a Gaussian distribution:  $\boldsymbol{\mu}_c^{\text{ood}} \sim \mathcal{N}(\mathbf{0}, \sigma_s^2)$ . Then OOD test samples were generated from these new cluster centers:

$$p_{\text{ood}}(\mathbf{y}) = \frac{1}{C_{\text{ood}}} \sum_{c=1}^{C_{\text{ood}}} \mathcal{N}(\boldsymbol{\mu}_c^{\text{ood}}, \sigma_r^2 I). \quad (10)$$

To evaluate the model’s zero-shot performance, we evaluate  $C + 1$  way cluster identification analysis on the  $C$  training clusters and the one cluster to which each OOD test sample belongs. Similar to Figure 6c, we calculated the proportion of predicted features from test brain data that were correctly classified as belonging to the original cluster centers compared with the other candidate clusters. The similarity between predicted features and each cluster center was calculated using the correlation coefficient, with the highest similarity determining the cluster assignment, where the chance level is  $1/(C + 1)$ . We evaluated the cluster identification performance for each of the OOD clusters and reported the median performance. Note that, for in-distribution test samples, we also conducted a  $C + 1$  way identification analysis on the  $C$  training clusters and one selected OOD cluster for fair comparison.

In the simulation analysis, we mainly focused on the cluster identification performance for the dimension  $D$ , for the number of clusters in the training set  $C$  or the distance among cluster centers for large sample size  $N = 500000$ . Other parameters fixed in this simulation analysis as follows:  $\sigma_r^2 = 10/D$ ,  $\sigma_s^2 = 100/D$ ,  $\bar{\mathbf{A}}_{ij} \sim \mathcal{N}(0, D^{-1/2})$ ,  $\sigma_n^2 = 0.1$ ,  $\lambda = 1.0$ , and  $C_{\text{ood}} = 32$ . We parameterized the scale of the variances ( $\sigma_r^2$  and  $\sigma_s^2$ ) and the teacher weights  $\bar{\mathbf{A}}$  using the dimension  $D$  so that the order of magnitude of the output invariant from the dimension.

#### 4.5 Recovery check of a single layer by iCNN

We performed a recovery check analysis using a single layer from the iCNN method at Figure 10. Briefly, the iCNN method generates an image by optimizing pixel values to make the image’s latent features similar to the target latent features (Shen et al., 2019b). In the pixel optimization condition (the left columns of each recovery image in Figure 10), we directly optimized the pixel values of images to minimize the mean squared loss between the latent feature of the image as well as the total-variance (TV) loss of pixel values (Mahendran and Vedaldi, 2015).

Additionally, the iCNN method can incorporate image generator networks (middle and right columns of each recovery image in Figure 10) to add constraints on image statistics. Instead of optimizing the pixel values, we optimized the parameters related to the generator networks to minimize the mean squared loss between the latent features obtained through the generator networks and the target latent features. As a weak image prior, we used Deep image prior (DIP) (Ulyanov et al., 2017). DIP utilizes a hierarchical U-Net architecture as an inherent prior for image tasks, capturing the statistical regularities of images without relying on a specific dataset. This model works effectively by optimizing a randomly initialized neural network that can be used as an image prior in various inverse problems such as

denoising, super-resolution, and inpainting tasks. In our analysis, DIP started with a U-Net initialized with random noise. Subsequently, the latent features and parameters of DIP were optimized to minimize the difference between the network’s output and target DNN features. For the pretrained image prior, we used the same generator model as in Shen et al. (2019b) (Dosovitskiy and Brox, 2016), optimizing the latent features of the pretrained networks.

#### 4.6 Expected identification accuracy in imprecise reconstructions

A pairwise identification accuracy is a metric defined on three types of samples: the test sample, the predicted sample, and the candidate sample selected from a test set as  $\mathbf{y}, \hat{\mathbf{y}}, \mathbf{y}_- \in \mathcal{Y}$ , respectively. We define a function  $S: \mathcal{Y} \times \mathcal{Y} \times \mathcal{Y} \rightarrow \mathbb{R}$  that takes the aforementioned triplet as the input and output whether the predicted sample was much close to the test sample than the candidate sample as

$$S(\hat{\mathbf{y}}, \mathbf{y}, \mathbf{y}_-) = \begin{cases} 1 & (\text{sim}(\hat{\mathbf{y}}, \mathbf{y}) \geq \text{sim}(\hat{\mathbf{y}}, \mathbf{y}_-)) \\ 0 & (\text{otherwise}) \end{cases} \quad (11)$$

where  $\text{sim}(\cdot, \cdot)$  is an arbitrary function that evaluates a similarity between two samples. The pairwise identification accuracy  $\text{Acc}$  over  $n$  test samples is defined as

$$\text{Acc} = \frac{1}{n(n-1)} \sum_i^n \sum_{j \neq i}^n S(\hat{\mathbf{y}}^{(i)}, \mathbf{y}^{(i)}, \mathbf{y}_-^{(i)}). \quad (12)$$

Now we consider a scenario where the translator only decodes semantic information (e.g., category) and cannot decode information about its precise visual appearance. Suppose the test set contains a categorical structure like NSD stimuli, we model such a scenario as

$$\mathbb{E}_{p(\mathbf{y}, \hat{\mathbf{y}}, \mathbf{y}_- | (\mathbf{y}, \hat{\mathbf{y}}, \mathbf{y}_-) \in Z)} [S(\hat{\mathbf{y}}, \mathbf{y}, \mathbf{y}_-)] = 0.5, \quad (13)$$

$$\mathbb{E}_{p(\mathbf{y}, \hat{\mathbf{y}}, \mathbf{y}_- | (\mathbf{y}, \hat{\mathbf{y}}, \mathbf{y}_-) \in \bar{Z})} [S(\hat{\mathbf{y}}, \mathbf{y}, \mathbf{y}_-)] = q \text{ where } q \in [0.5, 1]. \quad (14)$$

$Z$  is a set of triplet of which the test sample and the candidate sample belong to the same category.  $\bar{Z}$  is a complementary set of  $Z$ .  $\mathbb{E}_{p(\mathbf{y}, \hat{\mathbf{y}}, \mathbf{y}_- | \cdot)} [S(\hat{\mathbf{y}}, \mathbf{y}, \mathbf{y}_-)]$  represents the pairwise identification accuracy in the conditional expectation form. If the candidate sample belongs to the same category as the test sample, pairwise identification is challenging because of the poor prediction of the translator. On the other hand, if the candidate samples belongs to a different category than the test sample, the test sample is easily identified only from the semantic information.

Here, we assume that the test set contains  $k$  categories in total and all samples are equally distributed across each category for simplicity. If we have sufficiently large number of test samples, the above identification accuracy can be approximated as

$$\text{Acc} = \frac{1}{n(n-1)} \left( \sum_{(\mathbf{y}, \hat{\mathbf{y}}, \mathbf{y}_-) \in Z} S(\hat{\mathbf{y}}, \mathbf{y}, \mathbf{y}_-) \right) + \frac{1}{n(n-1)} \left( \sum_{(\mathbf{y}, \hat{\mathbf{y}}, \mathbf{y}_-) \in \bar{Z}} S(\hat{\mathbf{y}}, \mathbf{y}, \mathbf{y}_-) \right) \quad (15)$$

$$= \frac{|Z|}{n(n-1)} \left( \frac{1}{|Z|} \sum_{(\mathbf{y}, \hat{\mathbf{y}}, \mathbf{y}_-) \in Z} S(\hat{\mathbf{y}}, \mathbf{y}, \mathbf{y}_-) \right) + \frac{|\bar{Z}|}{n(n-1)} \left( \frac{1}{|\bar{Z}|} \sum_{(\mathbf{y}, \hat{\mathbf{y}}, \mathbf{y}_-) \in \bar{Z}} S(\hat{\mathbf{y}}, \mathbf{y}, \mathbf{y}_-) \right) \quad (16)$$

$$\stackrel{n \rightarrow \infty}{=} \frac{1}{k} \cdot \mathbb{E}_{p(\mathbf{y}, \hat{\mathbf{y}}, \mathbf{y}_- | (\mathbf{y}, \hat{\mathbf{y}}, \mathbf{y}_-) \in Z)} [S] + \left( 1 - \frac{1}{k} \right) \cdot \mathbb{E}_{p(\mathbf{y}, \hat{\mathbf{y}}, \mathbf{y}_- | (\mathbf{y}, \hat{\mathbf{y}}, \mathbf{y}_-) \in \bar{Z})} [S] \quad (17)$$

$$= \frac{1}{k} \cdot 0.5 + \left( 1 - \frac{1}{k} \right) \cdot q, \quad (18)$$

where  $|Z| = n(n/k - 1)$ , and  $|\bar{Z}| = n(n - n/k)$ . We used the assumption on the large sample size at the third equality.

## 5 Acknowledgements

We thank our laboratory team, especially Eizaburo Doi, Hideki Izumi, Matthias Mildenerger and for their invaluable comments and suggestions on the manuscript. This work was supported by the Japan Society for the Promotion of Science (JSPS: KAKENHI grants JP20H05954, JP20H05705 to Y.K., JP21K17821 to Y.N., and 22KJ1801 to K.S.), Japan Science and Technology Agency (JST: CREST grants JPMJCR18A5, and JPMJCR22P3 to Y.K.), and New Energy and Industrial Technology Development Organization (NEDO: commissioned project, JPNP20006 to Y.K.).

## References

- Emily Allen, Ghislain St-Yves, Yihan Wu, Jesse Breedlove, Jacob Prince, Logan Dowdle, Matthias Nau, Brad Caron, Franco Pestilli, Ian Charest, et al. A massive 7t fmri dataset to bridge cognitive neuroscience and artificial intelligence. *Nature neuroscience*, 25:116–126, 2022.
- Yunpeng Bai, Xintao Wang, Yan-pei Cao, Yixiao Ge, Chun Yuan, and Ying Shan. DreamDiffusion: Generating high-quality images from brain EEG signals. *arXiv preprint arXiv:2306.16934*, 2023.
- Roman Beliy, Guy Gaziv, Assaf Hoogi, Francesca Strappini, Tal Golan, and Michal Irani. From voxels to pixels and back: self-supervision in natural-image reconstruction from fmri. In *Proceedings of the 33rd International Conference on Neural Information Processing Systems*, volume 585. Curran Associates Inc., 2019.
- Yohann Benchetrit, Hubert Banville, and Jean-Rémi King. Brain decoding: toward real-time reconstruction of visual perception. *arXiv preprint arXiv:2310.19812*, 2024.
- Gijs Brouwer and David Heeger. Decoding and reconstructing color from responses in human visual cortex. *Journal of Neuroscience*, 29:13992–14003, 2009.
- Tom Brown, Benjamin Mann, Nick Ryder, Melanie Subbiah, Jared D Kaplan, Prafulla Dhariwal, Arvind Neelakantan, Pranav Shyam, Girish Sastry, Amanda Askell, et al. Language models are few-shot learners. In *Advances in Neural Information Processing Systems*, volume 33, pages 1877–1901. Curran Associates, Inc., 2020.
- Charlotte Caucheteux, Alexandre Gramfort, and Jean-Rémi King. Evidence of a predictive coding hierarchy in the human brain listening to speech. *Nature Human Behaviour*, 7:430–441, 2023.
- Zijiao Chen, Jiaxin Qing, Tiange Xiang, Wan Lin Yue, and Juan Helen Zhou. Seeing beyond the brain: Masked modeling conditioned diffusion model for human vision decoding. In *Proceedings of the IEEE/CVF Conference on Computer Vision and Pattern Recognition*, 2023a.
- Zijiao Chen, Jiaxin Qing, and Juan Helen Zhou. Cinematic mindscapes: High-quality video reconstruction from brain activity. *arXiv preprint arXiv:2306.16934*, 2023b.
- Fan Cheng, Tomoyasu Horikawa, Kei Majima, Misato Tanaka, Mohamed Abdelhack, Shuntaro Aoki, Jin Hirano, and Yukiyasu Kamitani. Reconstructing visual illusory experiences from human brain activity. *Science Advances*, 9:eadj3906, 2023.
- Rewon Child. Very deep VAEs generalize autoregressive models and can outperform them on images. In *International Conference on Learning Representations*, 2021.
- Devin Coldewey. Google’s best Gemini demo was faked, 2023. URL <https://techcrunch.com/2023/12/07/googles-best-gemini-demo-was-faked/>.
- Colin Conwell, Jacob Prince, Kendrick Kay, George Alvarez, and Talia Konkle. What can 1.8 billion regressions tell us about the pressures shaping high-level visual representation in brains and machines? *bioRxiv preprint bioRxiv:10.1101/2022.03.28.485868*, 2023.
- Jia Deng, Wei Dong, Richard Socher, Li-Jia Li, Kai Li, and Li Fei-Fei. ImageNet: A large-scale hierarchical image database. In *2009 IEEE Conference on Computer Vision and Pattern Recognition*, pages 248–255. IEEE, 2009.
- Timo Denk, Yu Takagi, Takuya Matsuyama, Andrea Agostinelli, Tomoya Nakai, Christian Frank, and Shinji Nishimoto. Brain2Music: Reconstructing music from human brain activity. *arXiv preprint arXiv:2307.11078*, 2023.
- Keyan Ding, Kede Ma, Shiqi Wang, and Eero Simoncelli. Image quality assessment: Unifying structure and texture similarity. *IEEE Transactions on Pattern Analysis and Machine Intelligence*, 44:2567–2581, 2020.
- Alexey Dosovitskiy and Thomas Brox. Generating images with perceptual similarity metrics based on deep networks. In *Advances in Neural Information Processing Systems*, volume 29, pages 658–666. Curran Associates, Inc., 2016.
- Matteo Ferrante, Furkan Ozcelik, Tommaso Boccato, Rufin VanRullen, and Nicola Toschi. Brain captioning: Decoding human brain activity into images and text. *arXiv preprint arXiv:2305.11560*, 2023.
- Stephanie Fu, Netanel Tamir, Shobhita Sundaram, Lucy Chai, Richard Zhang, Tali Dekel, and Phillip Isola. Dreamsim: Learning new dimensions of human visual similarity using synthetic data. *arXiv preprint arXiv:2306.09344*, 2023.
- Guy Gaziv, Roman Beliy, Niv Granot, Assaf Hoogi, Francesca Strappini, Tal Golan, and Michal Irani. Self-supervised natural image reconstruction and large-scale semantic classification from brain activity. *NeuroImage*, 253:119–121, 2022.
- Alessandro Gifford, Benjamin Lahner, Sari Saba-Sadiya, Martina Vilas, Alex Lascelles, Aude Oliva, Kendrick Kay, Gemma Roig, and Radoslaw Cichy. The algonauts project 2023 challenge: How the human brain makes sense of natural scenes. *arXiv preprint arXiv:2301.03198*, 2023.

- Uri Hasson, Samuel A. Nastase, and Ariel Goldstein. Direct fit to nature: An evolutionary perspective on biological and artificial neural networks. *Neuron*, 105:416–434, 2020.
- James Haxby, Swaroop Guntupalli, Andrew Connolly, Yaroslav Halchenko, Bryan Conroy, Ida Gobbini, Michael Hanke, and Peter Ramadge. A Common, high-dimensional model of the representational space in human ventral temporal cortex. *Neuron*, 72:404–416, 2011.
- James V. Haxby, M. Ida Gobbini, Maura L. Furey, Alumi Ishai, Jennifer L. Schouten, and Pietro Pietrini. Distributed and overlapping representations of faces and objects in ventral temporal cortex. *Science*, 293:2425–2430, 2001.
- Martin Hebart, Oliver Contier, Lina Teichmann, Adam Rockter, Charles Zheng, Alexis Kidder, Anna Corriveau, Maryam Vaziri-Pashkam, and Chris Baker. THINGS-data, a multimodal collection of large-scale datasets for investigating object representations in human brain and behavior. *eLife*, 12:e82580, 2023.
- Irina Higgins, David Amos, David Pfau, Sebastien Racaniere, Loic Matthey, Danilo Rezende, and Alexander Lerchner. Towards a definition of disentangled representations. *arXiv preprint arXiv:1812.02230*, 2018.
- Geoffrey Hinton and Russ Salakhutdinov. Reducing the dimensionality of data with neural networks. *Science*, 313: 504–507, 2006.
- Tomoyasu Horikawa and Yukiyasu Kamitani. Generic decoding of seen and imagined objects using hierarchical visual features. *Nature Communications*, 8:1–15, 2017.
- Tomoyasu Horikawa and Yukiyasu Kamitani. Attention modulates neural representation to render reconstructions according to subjective appearance. *Communications Biology*, 5:34, 2022.
- Tomoyasu Horikawa, Masako Tamaki, Youichi Miyawaki, and Yukiyasu Kamitani. Neural decoding of visual imagery during sleep. *Science*, 340:639–642, 2013.
- Yukiyasu Kamitani and Frank Tong. Decoding the visual and subjective contents of the human brain. *Nature Neuroscience*, 8:679–85, 2005.
- Isaak Kavasidis, Simone Palazzo, Concetto Spampinato, Daniela Giordano, and Mubarak Shah. Brain2image: Converting brain signals into images. In *Proceedings of the 25th ACM International Conference on Multimedia*, pages 1809–1817. Association for Computing Machinery, 2017.
- Kendrick Kay, Thomas Naselaris, Ryan Prenger, and Jack Gallant. Identifying natural images from human brain activity. *Identifying natural images from human brain activity*, 452:352–355, 2008.
- Diederik Kingma and Max Welling. Auto-encoding variational bayes. In *2nd International Conference on Learning Representations*, 2014.
- Naoko Koide-Majima, Shinji Nishimoto, and Kei Majima. Mental image reconstruction from human brain activity: Neural decoding of mental imagery via deep neural network-based Bayesian estimation. *Neural Networks*, 170: 349–363, 2024.
- Jonathan Kominsky, Kelsey Lucca, Ashley Thomas, Michael Frank, and Kiley Hamlin. Simplicity and validity in infant research. *Cognitive Development*, 63:101213, 2022.
- Nikolaus Kriegeskorte and Pamela Douglas. Interpreting encoding and decoding models. *Current Opinion in Neurobiology*, 55:167–179, 2019.
- Brenden Lake, Tomer Ullman, Joshua Tenenbaum, and Samuel Gershman. Building machines that learn and think like people. *Behavioral and Brain Sciences*, 40:e253, 2017.
- Yu-Ting Lan, Kan Ren, Yansen Wang, Wei-Long Zheng, Dongsheng Li, Bao-Liang Lu, and Lili Qiu. Seeing through the brain: Image reconstruction of visual perception from human brain signals. *arXiv preprint arXiv:2308.02510*, 2023.
- Hugo Larochelle, Dumitru Erhan, and Yoshua Bengio. Zero-data learning of new tasks. In *Proceedings of the 23rd national Conference on Artificial Intelligence*, volume 2, pages 646–651. National conference of Artificial Intelligence, 2008.
- Ren Li, Jared Johansen, Hamad Ahmed, Thomas Ilyevsky, Ronnie Wilbur, Hari Bharadwaj, and Jeffrey Siskind. Training on the test set? An analysis of Spampinato et al. [31]. *arXiv preprint arXiv:1812.07697*, 2018.
- Sikun Lin, Thomas Christopher Sprague, and Ambuj Singh. Mind reader: Reconstructing complex images from brain activities. In *Advances in Neural Information Processing Systems*. Curran Associates, Inc., 2022.
- Tsung-Yi Lin, Michael Maire, Serge Belongie, Lubomir Bourdev, Ross Girshick, James Hays, Pietro Perona, Deva Ramanan, Lawrence Zitnick, and Piotr Dollár. Microsoft COCO: Common objects in context. In *Computer Vision – ECCV 2014*, pages 740–755. Springer International Publishing, 2014.

- Aravindh Mahendran and Andrea Vedaldi. Understanding deep image representations by inverting them. In *2015 IEEE Conference on Computer Vision and Pattern Recognition*, pages 5188–5196. IEEE, 2015.
- Kei Majima, Paul Sukhanov, Tomoyasu Horikawa, and Yukiyasu Kamitani. Position information encoded by population activity in hierarchical visual areas. *eNeuro*, 4:224–231, 2017.
- Leland McInnes, John Healy, and James Melville. UMAP: Uniform Manifold Approximation and Projection for Dimension Reduction. *arXiv preprint arXiv:1802.03426*, 2018.
- Lisa Messeri and Molly Crockett. Artificial intelligence and illusions of understanding in scientific research. *Nature*, 627:49–58, 2024.
- Tom Mitchell, Svetlana Shinkareva, Andrew Carlson, Kai-Min Chang, Vicente Malave, Robert Mason, and Marcel Adam Just. Predicting human brain activity associated with the meanings of nouns. *Science*, 320:1191–1195, 2008.
- Yoichi Miyawaki, Hajime Uchida, Okito Yamashita, Masa-aki Sato, Yusuke Morito, Hiroki Tanabe, Norihiro Sadato, and Yukiyasu Kamitani. Visual image reconstruction from human brain activity using a combination of multiscale local image decoders. *Neuron*, 60:915–929, 2008.
- Milad Mozafari, Leila Reddy, and Rufin VanRullen. Reconstructing natural scenes from fMRI patterns using BigBiGAN. In *International Joint Conference on Neural Networks*, pages 1–8. IEEE, 2020.
- Tomoya Nakai, Naoko Koide-Majima, and Shinji Nishimoto. Correspondence of categorical and feature-based representations of music in the human brain. *Brain and Behavior*, 11:e01936, 2021.
- Thomas Naselaris, Emily Allen, and Kendrick Kay. Extensive sampling for complete models of individual brains. *Current Opinion in Behavioral Sciences*, 40:45–51, 2021.
- Samuel Nastase, Ariel Goldstein, and Uri Hasson. Keep it real: rethinking the primacy of experimental control in cognitive neuroscience. *NeuroImage*, 222:117254, 2020.
- Shinji Nishimoto, An Vu, Thomas Naselaris, Yuval Benjamini, Bin Yu, and Jack Gallant. Reconstructing visual experiences from brain activity evoked by natural movies. *Current Biology*, 21:1641–1646, 2011.
- Taiki Orima, Suguru Wakita, and Isamu Motoyoshi. Decoding and reconstruction of surface materials from EEG. *arXiv preprint arXiv:2309.05922*, 2024.
- Furkan Ozcelik and Rufin VanRullen. Natural scene reconstruction from fMRI signals using generative latent diffusion. *Scientific Reports*, 13:156–166, 2023.
- Furkan Ozcelik, Bhavin Choksi, Milad Mozafari, Leila Reddy, and Rufin VanRullen. Reconstruction of perceived images from fMRI patterns and semantic brain exploration using instance-conditioned GANs. In *International Joint Conference on Neural Networks*, 2022.
- Mark Palatucci, Dean Pomerleau, Geoffrey Hinton, and Tom Mitchell. Zero-shot learning with semantic output codes. In *Advances in Neural Information Processing Systems*, volume 22, pages 1410–1418. Curran Associates, Inc., 2009.
- Jacob Prince, Ian Charest, Jan Kurzwski, John Pyles, Michael Tarr, and Kendrick Kay. Improving the accuracy of single-trial fMRI response estimates using GLMsingl. *eLife*, 11:e77599, 2022.
- Kai Qiao, Jian Chen, Linyuan Wang, Chi Zhang, Li Tong, and Bin Yan. BigGAN-based bayesian reconstruction of natural images from human brain activity. *Neuroscience*, 444:92–105, 2020.
- Jon Raasch. ‘Mind reading,’ restoring vision to the blind and giving the deaf hearing could be possible: Neurosurgeon, 2023. URL <https://www.foxnews.com/us/mind-reading-restoring-vision-blind-giving-deaf-hearing-possible-neurosurgeon>.
- Alec Radford, Jong Wook Kim, Chris Hallacy, Aditya Ramesh, Gabriel Goh, Sandhini Agarwal, Girish Sastry, Amanda Askell, Pamela Mishkin, Jack Clark, Gretchen Krueger, and Ilya Sutskever. Learning transferable visual models from natural language supervision. In *Proceedings of the 38th International Conference on Machine Learning*, volume 139, pages 8748–8763. PMLR, 2021.
- Aditya Ramesh, Mikhail Pavlov, Gabriel Goh, Scott Gray, Chelsea Voss, Alec Radford, Mark Chen, and Ilya Sutskever. Zero-Shot text-to-image generation. In *Proceedings of the 38th International Conference on Machine Learning*, volume 139, pages 8821–8831. PMLR, 2021.
- Vipula Rawte, Amit Sheth, and Amitava Das. A survey of hallucination in large foundation models. *arXiv preprint arXiv:2309.05922*, 2023.
- Ziqi Ren, Jie Li, Xuetong Xue, Xin Li, Fan Yang, Zhicheng Jiao, and Xinbo Gao. Reconstructing seen image from brain activity by visually-guided cognitive representation and adversarial learning. *NeuroImage*, 226:117593, 2021.

- Robin Rombach, Andreas Blattmann, Dominik Lorenz, Patrick Esser, and Björn Ommer. High-resolution image synthesis with latent diffusion models. In *Proceedings of the IEEE/CVF Conference on Computer Vision and Pattern Recognition*, pages 10684–10695, 2022.
- Simon Schug, Maciej Wołczyk, Razvan Pascanu, and Seijin Kobayashi. Discovering modular solution that generalize compositionality. In *The Twelfth International Conference on Learning Representations*, 2024.
- Christoph Schuhmann, Romain Beaumont, Richard Vencu, Cade Gordon, Ross Wightman, Mehdi Cherti, Theo Coombes, Aarush Katta, Clayton Mullis, Mitchell Wortsman, et al. LAION-5B: An open large-scale dataset for training next generation image-text models. *arXiv preprint arXiv:2210.08402*, 2022.
- Paul Scotti, Atmadeep Banerjee, Jimmie Goode, Stepan Shabalin, Alex Nguyen, Cohen Ethan, Aidan James Dempster, Nathalie Verlinde, Elad Yundler, David Weisberg, et al. Reconstructing the mind’s eye: fMRI-to-image with contrastive learning and diffusion priors. In *Advances in Neural Information Processing Systems*, volume 36, pages 24705–24728. Curran Associates, Inc., 2023.
- Katja Seeliger, Umut Güçlü, Luca Ambrogioni, Yağmur Güçlütürk, and Marcel van Gerven. Generative adversarial networks for reconstructing natural images from brain activity. *NeuroImage*, 181:775–785, 2018.
- Guohua Shen, Kshitij Dwivedi, Kei Majima, Tomoyasu Horikawa, and Yukiyasu Kamitani. End-to-end deep image reconstruction from human brain activity. *Frontiers in Computational Neuroscience*, 13:13–21, 2019a.
- Guohua Shen, Tomoyasu Horikawa, Kei Majima, and Yukiyasu Kamitani. Deep image reconstruction from human brain activity. *PLOS Computational Biology*, 15:e1006633, 2019b.
- Karen Simonyan and Andrew Zisserman. Very deep convolutional networks for large-scale image recognition. In *3rd International Conference on Learning Representations*, 2015.
- James Somers. The science of mind reading, 2021. URL <https://www.newyorker.com/magazine/2021/12/06/the-science-of-mind-reading>.
- Chun Soon, Marcel Brass, Hans Heinze, and John-Dylan Haynes. Unconscious determinants of free decisions in the human brain. *Nature Neuroscience*, 11:543–545, 2008.
- Garrett Stanley, Fei Fei. Li, and Yang Dan. Reconstruction of natural scenes from ensemble responses in the lateral geniculate nucleus. *The Journal of Neuroscience*, 19:8036–8042, 1999.
- Yu Takagi and Shinji Nishimoto. Improving visual image reconstruction from human brain activity using latent diffusion models via multiple decoded inputs. *arXiv preprint arXiv:2306.11536*, 2023a.
- Yu Takagi and Shinji Nishimoto. High-resolution image reconstruction with latent diffusion models from human brain activity. In *Proceedings of the IEEE/CVF Conference on Computer Vision and Pattern Recognition*, pages 14453–14463, 2023b.
- Jerry Tang, Amanda LeBel, Shailee Jain, and Alexander Huth. Semantic reconstruction of continuous language from non-invasive brain recordings. *Nature Neuroscience*, 26:858–866, 2023.
- Dmitry Ulyanov, Andrea Vedaldi, and Victor Lempitsky. Deep image prior. *arXiv preprint arXiv:1711.10925*, 2017.
- UNESCO. Unveiling the neurotechnology landscape. Scientific advancements innovations and major trends. *UNESCO*, 2023. URL <https://unesdoc.unesco.org/ark:/48223/pf0000386137>.
- Aaron van den Oord, Oriol Vinyals, and Koray Kavukcuoglu. Neural discrete representation learning. In *Advances in Neural Information Processing Systems*, volume 30, pages 6306–6315. Curran Associates, Inc., 2017.
- David C. Van Essen, Kamil Ugurbil, Erich Auerbach, Deanna Barch, Timothy Behrens, Robert Bucholz, Maurizio Corbetta, Steve Curtiss, Sam Della Penna, Deen Feinberg, et al. The human connectome project: A data acquisition perspective. *NeuroImage*, 62:2222–2231, 2012.
- Haibao Wang, Jun Kai Ho, Fan Cheng, Shuntaro Aoki, Yusuke Muraki, Misato Tanaka, and Yukiyasu Kamitani. Inter-individual and inter-site neural code conversion and image reconstruction without shared stimuli. *arXiv preprint arXiv:2403.11517*, 2024.
- Oliver Whang. A.I. is getting better at mind-reading, 2023. URL <https://www.nytimes.com/2023/05/01/science/ai-speech-language.html>.
- Jonathan Xu, Bruno Aristimunha, Max Emanuel Feucht, Emma Qian, Charles Liu, Tazik Shahjahan, Martyna Spyra, Steven Zifan Zhang, Nicholas Short, Jioh Kim, et al. Alljoined – A dataset for EEG-to-image decoding. *arXiv preprint arXiv:2404.05553*, 2024.
- Xingqian Xu, Zhangyang Wang, Eric Zhang, Kai Wang, and Humphrey Shi. Versatile diffusion: Text, images and variations all in one diffusion model. *arXiv preprint arXiv: 2211.08332*, 2022.



- Kentaro Yamada, Yoichi Miyawaki, and Yukiyasu Kamitani. Inter-subject neural code converter for visual image representation. *NeuroImage*, 113:289–297, 2015.
- Kechen Zhang and Terrence J. Sejnowski. Neuronal tuning: To sharpen or broaden? *Neural Computation*, 11:75–84, 1999.
- Qiongyi Zhou, Changde Du, Shengpei Wang, and Huiguang He. Clip-mused: Clip-guided multi-subject visual neural information semantic decoding. *ArXiv preprint arXiv:2402.08994*, 2024.

## A Supplementary figures

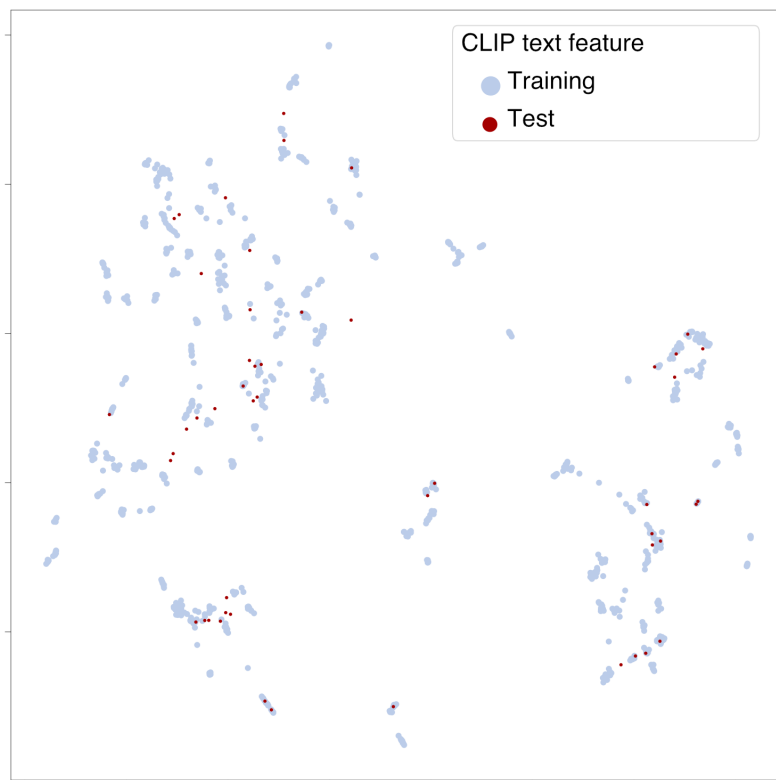


Figure S1: UMAP visualization of CLIP text features in Deeprecon. Blue points represent training samples, while red points represent test samples.

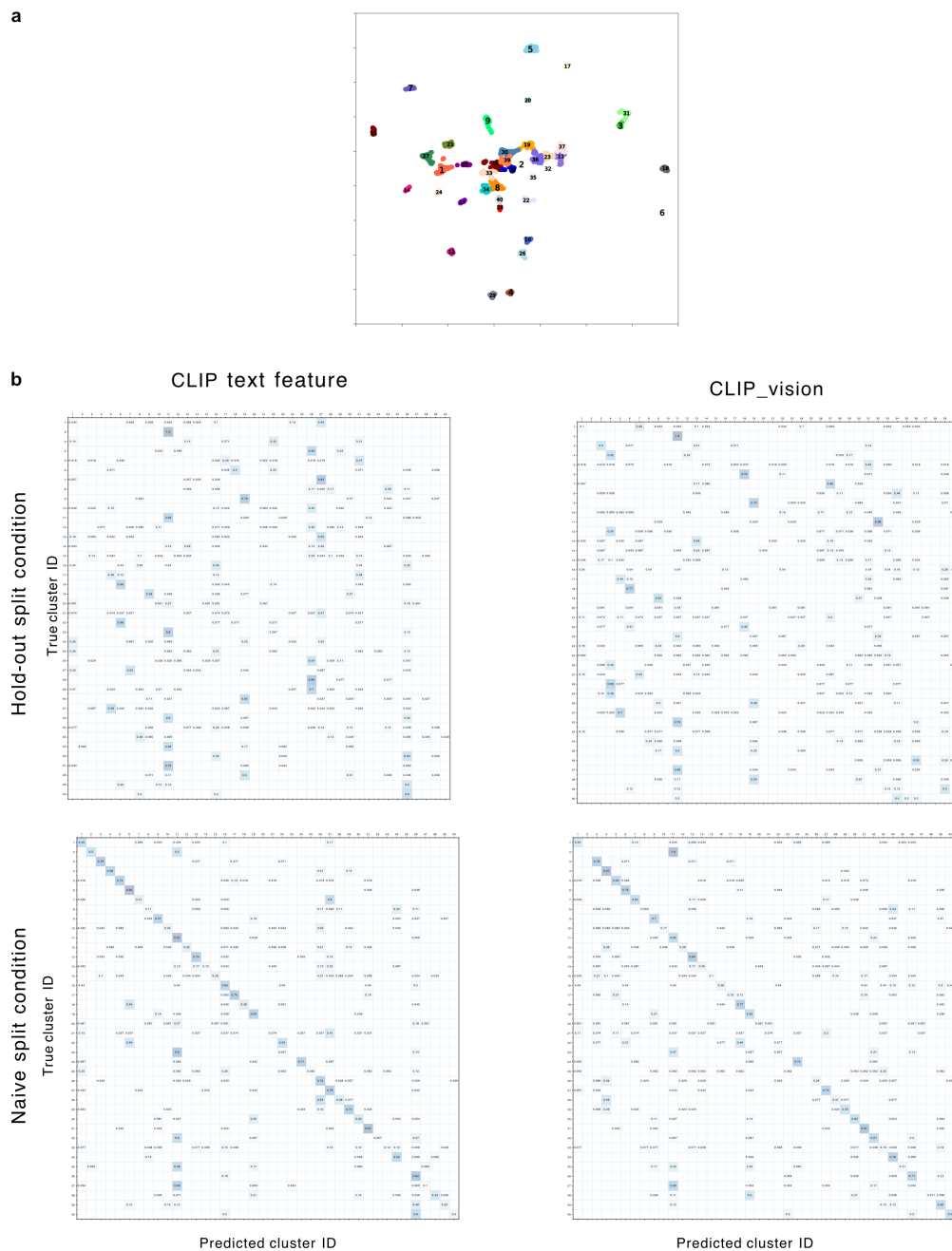


Figure S2: Supplementary information of hold out analysis. (a) The clustering results, applying the  $k$ -Means clustering to the UMAP embedding of CLIP text features. Based on these clustering results, the assignment of training and test samples under the hold-out split condition was determined. (b) Confusion probability matrix of cluster identification results. The top row shows the cluster identification results under the hold-out split conditions. The left side is for CLIP text features and the right side is for CLIP vision features. The bottom row shows the cluster identification results under the naive split conditions. In each matrix, the  $(i, j)$  cell indicates the ratio of samples assigned by cluster  $i$  are predicted to cluster  $j$ . The empty cell means the ratio is 0.

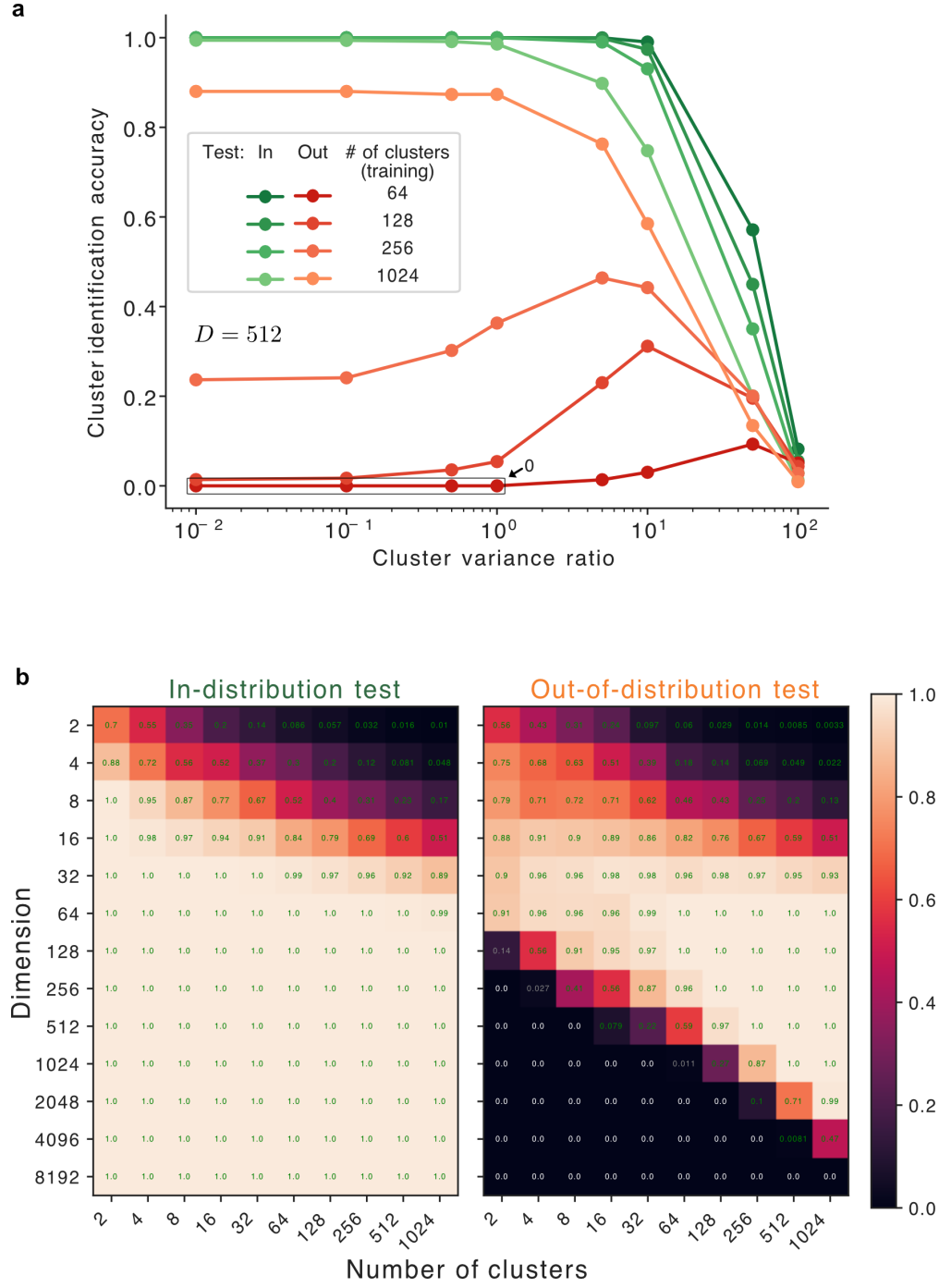


Figure S3: Additional results about simulation with clustered data. (a) Cluster identification accuracy as a function of the cluster variance ratio. The  $x$  axis indicates the cluster variance ratio  $\sigma_r^2/\sigma_s^2$  and the  $y$  axis represents the cluster identification performance. Green lines show the results of in-distribution test samples and orange lines show those for OOD samples. The number of clusters used in training is increasing as the color lightens. Similar to Figure 9b in the main figure, the OOD identification performance become closer to the in distribution samples as the cluster variance ratio is increasing. (b). Heatmap plot of cluster identification accuracy varying the number of clusters in training and dimension. The left matrix shows the cluster identification results for the in-distribution test samples. The right matrix shows the cluster identification results for the OOD test samples. In each matrix, the  $(i,j)$  cell indicates the cluster identification accuracy when the dimension is  $i$  and the number of clusters used in the training is  $j$ .

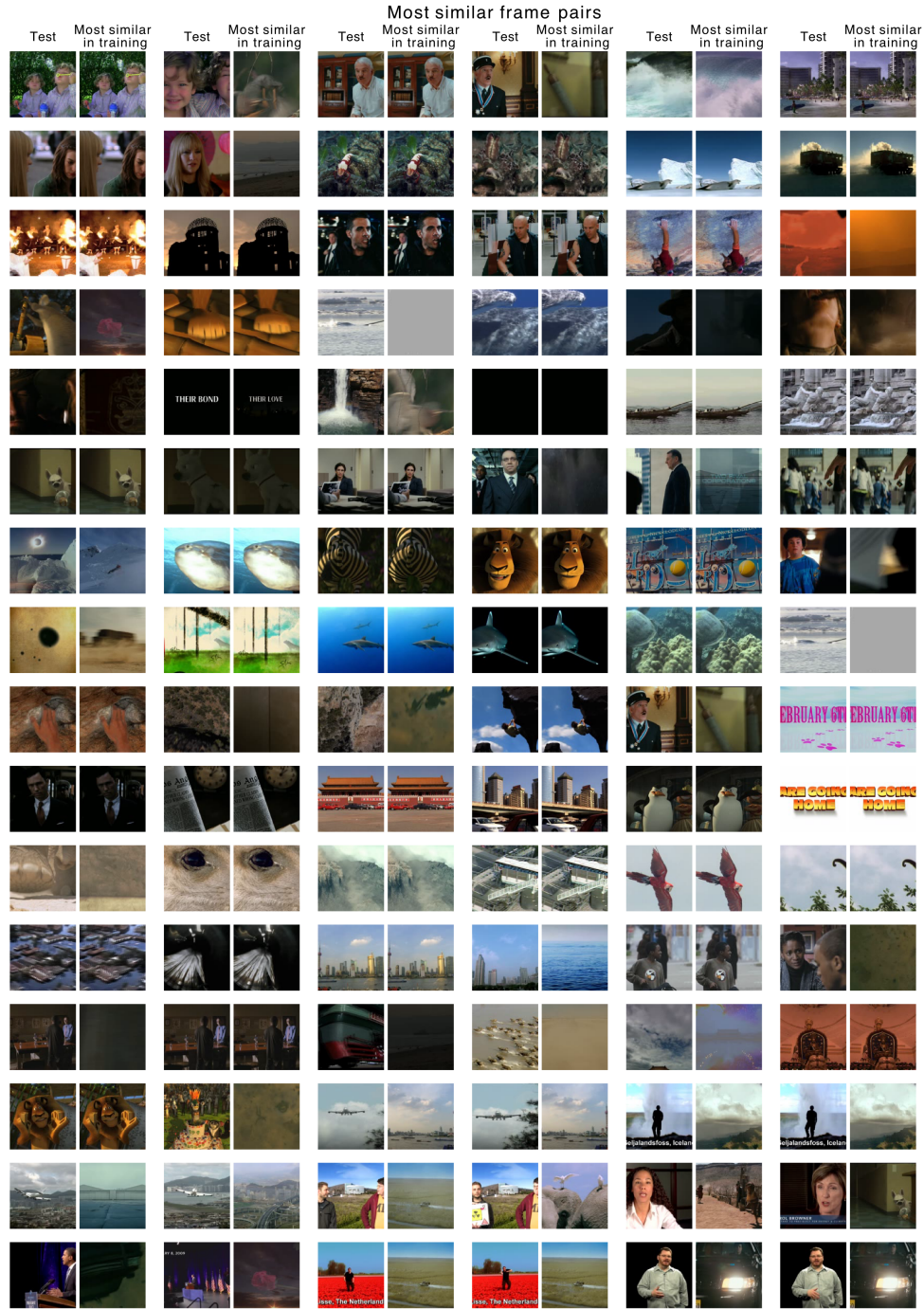


Figure S4: Frame similarity in Nishimoto et al. (2011). We first detected scenes from the training and test movie stimuli. Then, for the first and last frames of each test scene, we searched for the frame from the training movies with the closest Euclidean distance. Our analysis revealed that 37 out of the 48 scenes in the test set contained frames that were nearly identical to those in the training set.